ISSN 1028-8546

Volume XXII, Number 4
Section: En
December, 2016

Azerbaijan Journal of Physics

Fizika

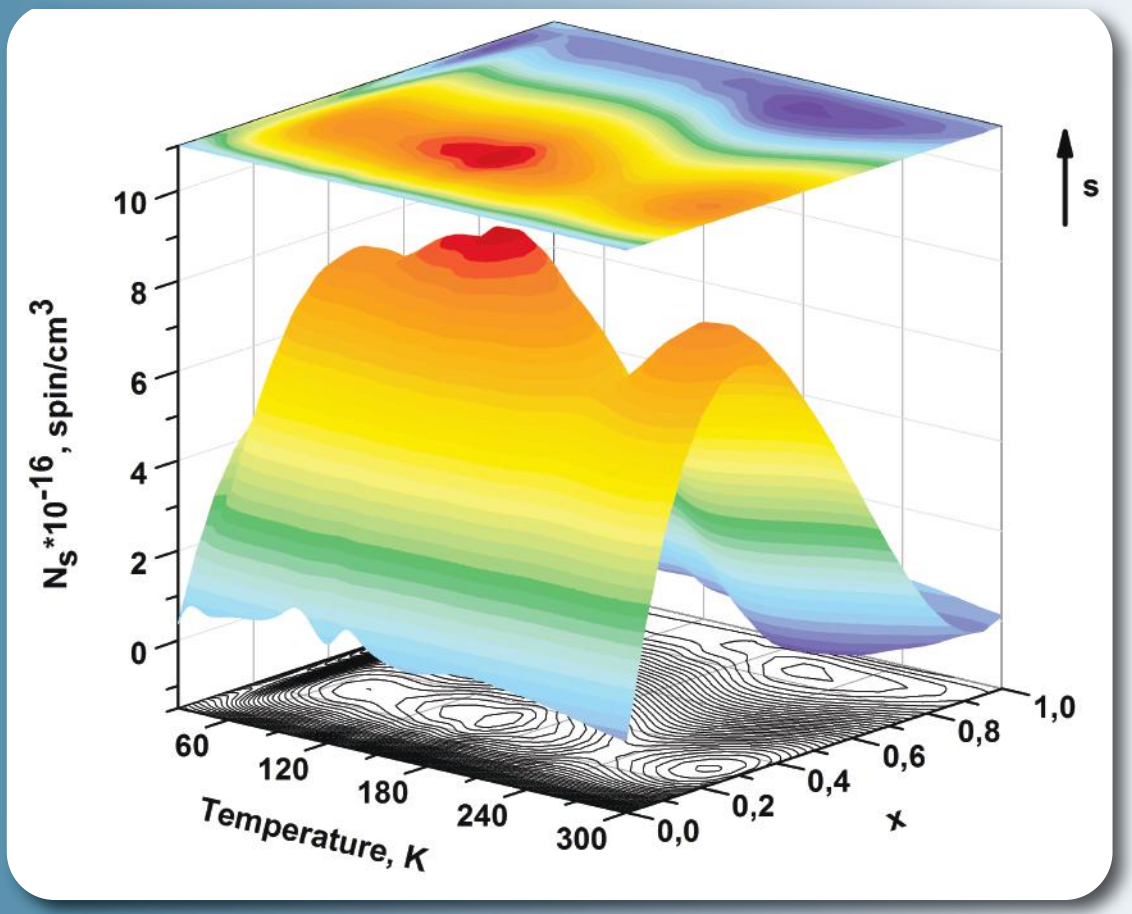

www.physics.gov.az

G.M. Abdullayev Institute of Physics
Azerbaijan National Academy of Sciences
Department of Physical, Mathematical and Technical Sciences

Published from 1995
Ministry of Press and Information
of Azerbaijan Republic,
Registration number 402, 16.04.1997

ISSN 1028-8546
vol. XXII, Number 04, 2016
Series: En

Azerbaijan Journal of Physics

FIZIKA

G.M.Abdullayev Institute of Physics
Azerbaijan National Academy of Sciences
Department of Physical, Mathematical and Technical Sciences

PUBLISHING OFFICE

131 H.Javid ave, AZ-1143, Baku
ANAS, G.M.Abdullayev Institute of Physics

Tel.: (99412) 539-51-63, 539-32-23
Fax: (99412) 447-04-56
E-mail: jophphysics@gmail.com
Internet: www.physics.gov.az

It is authorized for printing:

Published at "**SƏRQ-QƏRB**"
17 Ashug Alessger str., Baku
Typographer : Aziz Gulaliyev

Sent for printing on: __.__. 201_
Printing approved on: __.__. 201_
Physical binding:_____
Number of copies:_____200
Order:_____

CONFOCAL RAMAN MAPPING OF THE TOPMOST LAYER HETEROEPITAXIAL $InAs_{1-x}Sb_x$ STRUCTURES

Y.N. ALIYEVA[1], G. KIPSHIDZE[2], V.A. TANRIVERDIYEV[1], N.A. ABDULLAYEV[1], I.A. MAMEDOVA[1], N.T. MAMEDOV[1], A.A. SADIKHOVA[1]

[1]Institute of Physics, 131, G.Javid pr., Az-1143 Baku, Azerbaijan

[2]Stony Brook University, Stony Brook, New York, 11794, USA

The spectra of Raman scattering (RS) in surface epi-layer of $InAs_{1-x}Sb_x$ heteroepitaxial structure in more than 200 points on 50μm·50μm square by the means of the step-by-step scanning of focused laser beam on the surface layer (mapping) are investigated. The two-mode reconstruction of phonon spectrum in $InAs_{1-x}Sb_x$ solid solution is revealed. It is shown that such characteristics of spectral lines as the peak position and FWHM of spectral lines are identical in mainly points, that shows on the crystallinity and high degree of homogeneity of the obtained structures. Mapping is made for two more intensive spectral lines in RS (cadmium, mercury, stibium) spectrum of $InAs_{1-x}Sb_x$ solid solution thin films 187 cm^{-1}(InSb-like LO mode) and 222 cm^{-1} (InAs-like LO mode).

Keywords: Raman spectroscopy, optical phonons, epi-layer, heteroepitaxial structures, scanning, thin-film, Full width at half maximum (FWHM), homogeneity.

PACS: 78.30._ j

INTRODUCTION

$InAs_{1-x}Sb_x$ solid solutions have the unique property of wide range variation of the forbidden band width on the composition (x value). As it is known the forbidden band width of semiconductor compound InAs is E_{g0}=407,4meV and InSb is E_{g0}=227,3meV at temperature 77K [1]. The forbidden band width in $InAs_{1-x}Sb_x$ solid solutions slowly changes decreasing with Sb atom concentration increasing. The forbidden band width achieves the minimum value and can be the less than even in InSb achieving the value 100meV at Sb atom concentrations close to 60%(x=0,6) [2,3]. This fact is the most interesting. This unusual property is actively used nowadays for the development of optoelectronic devices (sources and radiation detectors) in technologically important spectrum range from 8 μm up to 12 μm in which the atmospheric windows are situated.

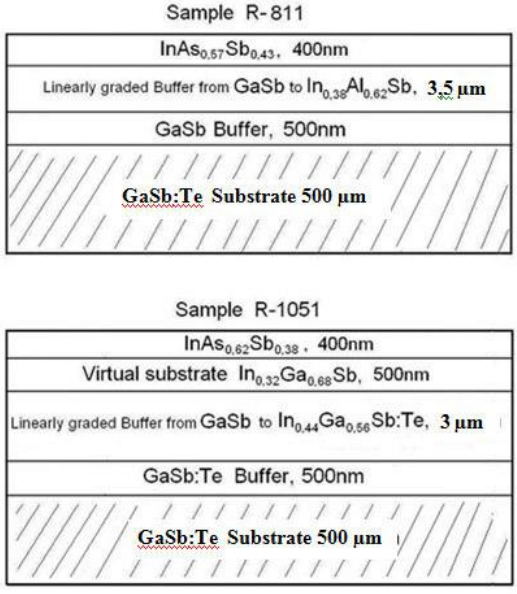

Fig. 1. The composition and thicknesses of heteroepitaxial structures $InAs_{0.57}Sb_{0.43}$ (sample R811) and $InAs_{0,62}Sb_{0,38}$ (sample R1051).

The absence of substrates with close values of the lattice constant is the main constraint for the obtaining and the wide application of thin-film photoelectronic devices (in particular, on the base of $InAs_{1-x}Sb_x$ solid solutions). The difference of lattice constants of work layer and substrate is the reason of appearance of the film stress and deformations leading to the formation of big density of defects and dislocations influencing on the main physical parameters and consistency of photoelectronic device operation. The lattice constants of GaSb and InSb are equal to 6,096 and 6,479Å correspondingly [1], i.e. the irrelevance is more than 6%. This irrelevance for epitaxy of $InAs_{1-x}Sb_x$ pseudomorphic solid solutions is gradually eliminated by us by application of intermediate step buffer layers (Al, Ga, In) (As, Sb). Thus, we obtain the unrelaxed and unstrained $InAs_{1-x}Sb_x$ top epi-layers. The characteristics (composition and widths of the layers) of obtained multilayer epitaxial heterostructures $InAs_{1-x}Sb_x$ for compositions with x=0,43 (sample R811) and x=0,38 (sample R1051) are shown in fig.1.

The identification of phonon spectrum reconstruction character in thin structures of $InAs_{1-x}Sb_x$ solid solutions and homogeneity degree of $InAs_{1-x}Sb_x$ top epi-layers is the main goal of the present paper.

RAMAN SCATTERING

It is well known that two RS active phonons, which are longitudinal optical phonons (LO) and transversal ones (TO,) are characteristics for crystals of $A^{III}B^{V}$ group with cubic lattice. According to [4] the frequency of LO phonon is 242cm^{-1} and one of TO phonon is 220cm^{-1} in InAs bulk single crystals; frequency of LO phonon is 193 cm^{-1} and one of TO phonon is 185cm^{-1} in InSb.

The RS investigations in heteroepitaxial structures R811 ($InAs_{0.57}Sb_{0.43}$) and R1051 ($InAs_{0.62}Sb_{0.38}$) on confocal Raman spectrometer “Nanofinder 30” (Tokyo Instr., Japan) are carried out by us. The investigations are carried out in backscattering geometry. YAG:Nd laser with second harmonic wavelength λ = 532 nm is used as

131 H.Javid ave, AZ-1143, Baku
ANAS, G.M.Abdullayev Institute of Physics
E-mail: jophphysics@gmail.com

excitation light source. The cooling CCD-camera (-70ºC) working in the regime of photon counting is served as radiation collector, the exposure time is usual 5 min, the radiation power incident on sample is 7-9mVt, and the beam diameter is near 4 μm. The diffraction lattice having 1800 dashes per millimeter is used in spectrometer, the determination accuracy of line spectral position is not worth 0,5 cm^{-1} is used in spectrometer.

The penetration depth of laser radiation and therefore the analysis effective depth at Raman scattering can be defined from ratio $\lambda/2\pi k$ where k is extinction factor. At InAsSb system analysis by the laser with wavelength λ = 532 nm such depth is approximately near 100nm with taking into consideration the extinction factor for InAs and InSb [5]. This fact shows that using the laser given wavelength for Raman scattering, we get the information only from top layer of the investigated multi-layer covering. According to selection rules obtained from analysis of Raman scattering tensors with diamond structure at backscattering from (100) surface, the only LO phonons can be observed and the appearance of TO ones is prohibited.

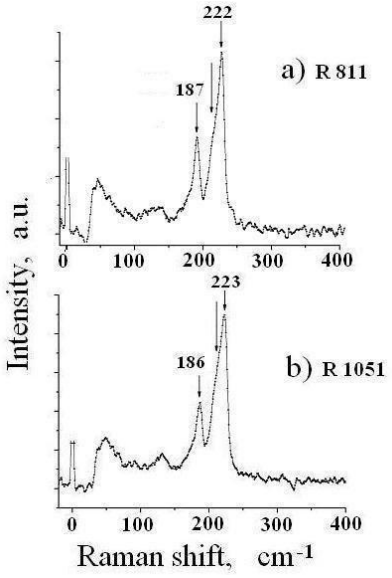

Fig. 2. Raman scattering spectra of samples R811 (a) and R1051 (b).

Raman scattering spectra in the backscattering regime at room temperature are shown in fig.2. It is obvious that the two-mode type of phonon spectrum reconstruction is character for $InAs_{1-x}Sb_x$ solid solution. The two-mode behavior of optical phonons is also established in work [6] by data of Raman scattering on $InAs_{1-x}Sb_x$ ($0 \le x \le 1$) solid solution thin films grown up on GaAs substrates by molecular-beam epitaxy method. The several phonon bands are observed in fig.2. These are: the intensive phonon band on frequencies 187 cm^{-1} ($InAs_{0,57}Sb_{0,43}$) and 186 cm^{-1} ($InAs_{0,62}Sb_{0,38}$) corresponding to longitudinal optical phonon in InSb (InSb-like LO) which is allowed band by selection rules for the given scattering geometry and asymmetric wide phonon one on 223 cm^{-1} ($InAs_{0,62}Sb_{0,38}$) presenting itself the overlapping of two bands of optical longitudinal and transversal phonons in InAs (InAs-like LO and InAs-like TO). This fact in given geometry Raman investigations of TO-phonons is the consequence of symmetry breaking of crystal lattice of epitaxial film as a result of disordering in solid state crystal lattice and small deviation comparison from backscattering geometry. It is necessary to note the high quality of GaSb bulk substrate differing by narrow spectral lines with FWHM of about 3cm^{-1} (fig.3). The frequency position corresponds to LO (235 cm^{-1}) and TO (226 cm^{-1}) RS active phonons in GaSb [4].

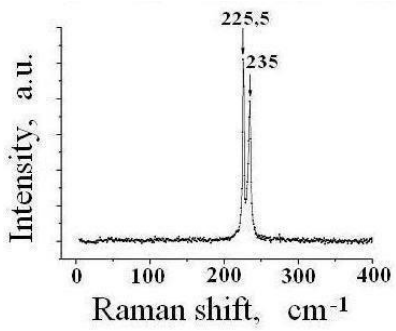

Fig. 3. Raman scattering spectra from GaSb substrate.

It is seen that the frequency 222 cm^{-1} shifts to the sides of bigger ones, i.e. to the frequences of KP active phonons character for InAs, as far as Sb atom number decrease in в $InAs_{1-x}Sb_x$ (sample R1051). The nature of observable less intensive wide bands at ~140 cm^{-1} isn't established and the additional investigations are required.

In work [6] it is experimentally established that frequences of LO and TO phonons in dependence on x composition in $InAs_{1-x}Sb_x$ solid solution change linearly as follows:

InAs-like LO	ν_{L1} (cm^{-1}) = 238–32x
InAs-like TO	ν_{T1} (cm^{-1}) = 219–27x
InSb-like LO	ν_{L2} (cm^{-1}) = 177+12x

The high homogeneity of obtained heteroepitaxial structures is approved by investigation data of micro-RS spectra by the way of laser beam scanning on structure surface (50μm·50μm) in mapping regime. Confocal raman mapping is an highly suitable analytical tool for the study of advanced materials such as heteroepitaxial $InAs_{1-x}Sb_x$ structures.

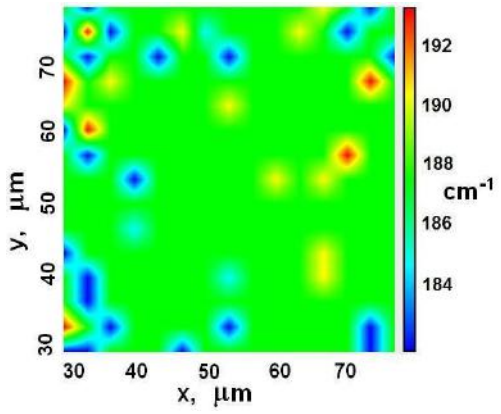

Fig. 4. Mapping of peak position of spectral line 187 cm^{-1}.

In mapping regime one can carry out the operation with each line emphasized from spectral ones by several characteristics: peak position of spectral lines, FWHM of spectral line, value of maximum intensity of spectral line, value of integrated intensity of spectral line and etc.

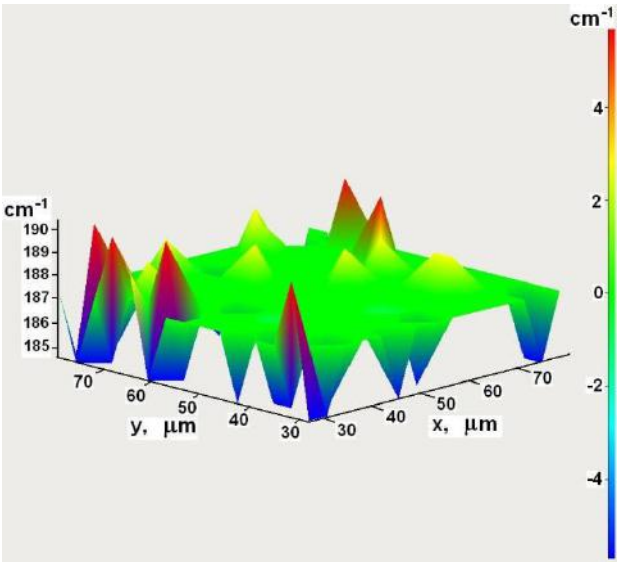

Fig. 5. Three-dimensional mapping image of peak position of spectral line 187 cm^{-1}.

The results of mapping peak position of spectral line 187 cm^{-1} in square 50µm·50µm are given in fig.4. The figure 4 gives the information approximately from 215 points (in 15 points in each direction). The peak position of spectral line in each coordinate point can be known by color ruler (on the right). For example, the areas painted in green color correspond to peak position of spectral line at 187-188 cm^{-1}, yellow and blue colors correspond to peak position at 190 and 184 cm^{-1}. Only very thin blue and red colors testify to presence of defects leading to peak position at 183 and 192 cm^{-1}. The three-dimensional visual mapping image is shown in fig.5.

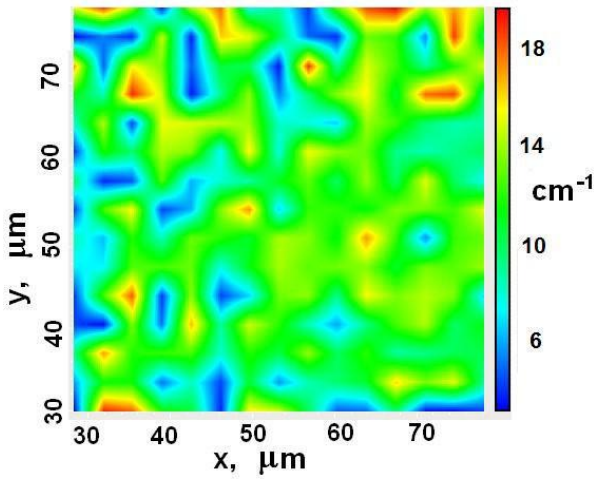

Fig. 6. Mapping of FWHM of spectral line 187 cm^{-1}.

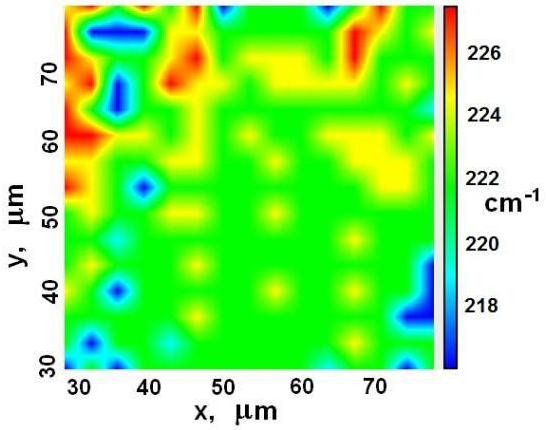

Fig. 7. Mapping of peak positions of spectral line 222cm^{-1}.

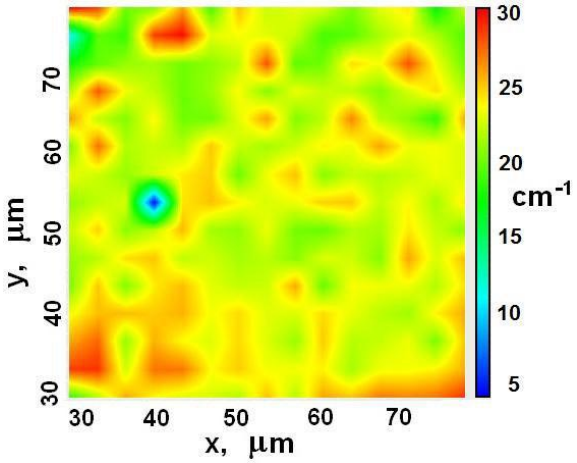

Fig. 8. Mapping of FWHM of spectral line 222 cm^{-1}.

The results of FWHM mapping (Full width at half maximum) of spectral line187cm^{-1} are given in fig.6. As it is seen FWHM mapping of spectral line 187cm^{-1} also testifies to homogeneity: the most part painted in green-bluish color shows that FWHM of spectral line 187 cm^{-1} is equal to 9-13 cm^{-1}.

The results of mapping peak position of spectral line 222 cm^{-1} are given in fig.7.The results of FWHM mapping of spectral line 222 cm^{-1} are given in fig.8, which also testify to high homogeneity of obtained heteroepitaxial structures $InAs_{1-x}Sb_x$.

CONCLUSION

The data of confocal Raman spectroscopy authenticate on two-mode type of phonon spectrum reconstruction in $InAs_{1-x}Sb_x$ solid solutions. The investigations in mapping regime testify tohomogeneity of obtained heteroepitaxial structures $InAs_{1-x}Sb_x$.

The investigations was supported by the Science Development Foundation under the President of the Republic of Azerbaijan (grant EIF-2013-9(15)-46/06/1).

[1] *I. Vurgaftman, J.R. Meyer, and L.R. Ram-Mohan*. J. Appl. Phys., **89**, 5815 (2001).
[2] *Z.M. Fang, K.Y. Ma, D.H.Jaw, R.M. Cohen and G.B. Stringfellow*. J. Appl. Phys., **67,** 7034 (1990).
[3] *M.Y. Yen, R. People, K.W. Wecht and A.Y. Cho*. Appl. Phys. Lett., **52**, 489 (1988).
[4] *M. Razeghi.* Eur. Phys. J. Appl. Phys., **23**, 149 (2003).
[5] *D.E.Aspnes, A.A. Studna.* Phys. Rev. B, **27**, 985 (1983).
[6] *Y.B. Li, S.S. Dosandjh, I.T. Ferguson, A.G. Norman, A.G. de Oliveyra, R.A. Stradling, R. Zallen.* Semicond. Sci. Technol.**7**, 567 (1992).

Received: 16.09.2016

DIELECTRIC PROPERTIES OF PP AND PP+DK_1 NANO-COMPOSITES IN DIFFERENT PERCENTAGE

A.A. KHADIYEVA, H.S. IBRAGIMOVA, V.A. ALEKPEROVA, A.R. SADIGOVA
Institute of Physics Academy of Sciences of Azerbaijan,
H.Javid ave. 33, AZ-1143 Baku
hicran90@rambler.ru

The dielectric properties of pure PP and PP+DK_1nano-composites researched in alternating electric field are presented in the given paper. It is revealed that dielectric properties change in the dependence on field frequency and temperature and also on filler concentration. This is explained by relaxation losses which take place because of composite structural elements with mobility different degree and also with appearance of low-molecular impurities, for example with revealing of CO polar groups.

Keywords: nano-composite, polypropylene, nanogel, rest degree
Pacs: 79,60.Dp ;78.66.Li;78.30.Am

INTRODUCTION

The obtaining and investigation of nano-composites is of interest in nano-technology field in the latest works. The obtaining of new materials consisting of disperse fillers with size 1-100cm uniting the photoluminescent, magnetic and catalytic characteristics are perspective ones. The investigations in the field of obtaining and properties of nano-composite materials strongly increase. Such dielectric characteristics of PP+DK_1 nano-composites as electrical conduction, processes of relaxation and polarization in alternating currents aren't studied enough and that's why the study of these properties in high-temperature and frequency interval is of great interest.

THE EXPERIMENT TECHNIQUES AND TEST PREPARATION

The dielectric properties of PP+DK_1 nano-composites present in the given paper. The samples with thickness 140-170μm are used for measurement of dielectric properties in alternating electric field. The mixtures of PP and DK_1 powders are prepared in different component ratio and further the nano-composites in film form with further cooling are prepared from these mixtures by hot pressing at polymer matrix melting point under pressure 15MPa during 10 min.

The samples are obtained in different temperature-time crystallization regimes and especially by rapid cooling (RC) method in mixture ice-water with velocity 30 grad/min. RC samples are investigated by us. The samples for measurement of dielectric characteristics in alternating current are prepared in the disc form by diameter 20mm. The stable electric contact is supplied for electrodes from stainless steel by diameter 15mm applying the extruded electrodes from aluminum foil by thickness 7μm. The samples are put into cell with brake electrodes. Knowing the electrocapacity C and sample geometric sizes one can define the complex value of dielectric constant with the help of formula

$$C = \frac{\varepsilon\varepsilon_0 S}{d}$$

where C is electrocapacity of the samples, d is thickness, S is electrode thickness being on the surface, ε_0=8,85·10^{-12} is electric constant. The electric constant frequency changes from 25Hz up to 10^6 Hz and temperature changes from 20 up to 150℃. The obtained results are presented in the form of real and imaginary parts of dielectric constant $(\varepsilon, \varepsilon')$, tg$\delta$ dielectric loss on electric field frequency and temperature. The temperature dependences of ε on tgδ in obtained nano-composites at frequency 1 Hz are shown in fig.2. From the figure it is seen that ε increase in nano-composite PP+10%DK_1 (where ε =3,1) on 40% relatively pure PP (ε =2,0) is observed, ε for DK_1 filler is $\varepsilon = 2-8$ and $\varepsilon = 2$ in matrix [107]. Such dependence of ε on T in nano-composite is defined by Maxwell-Wagner polarization. The values of surface energy, system conduction and other parameters of dielectric characteristics are close to percolation threshold in dependence on filler concentration. ε decreases relatively pure PP in small concentrations. The clusters form the instability of phase interactions and particles in nano-gels in 2% filler content because of the difference in component surface energy. The surface of these clusters is less than sum surface of their component particles. The cluster number increases and dielectric layer between particles decreases with increase of filler volume content and this leads to increase of electric capacity (i.e. increase of ε). As it is seen from the figure 1 for composites PP+2%DK_1 ε doesn't change at temperature increasing 290-330K. But, $\varepsilon = f(T)$ dependence character changes at following addition increase in PP+10%DK_1 composite. Firstly, the dielectric constant increases with temperature increasing and the strong ε increase takes place in temperature interval of crystallite melting ($\sim 393K$), further ε doesn't change with temperature increasing. The temperature decrease on 15K in PP+10%DK_1 composites shifts to low-temperature region in comparison with pure polymer PP and PP+2%DK_1 composite. The dielectric losses significantly increase at consideration of tgδ change in dependence on temperature in PP+10%DK_1 composite (fig.2).

At temperature 293K for pure PP $tg\delta$ is 0,007±0,001 and 0,025±0,001 is for PP+10%DK_1. The significant value of dielectric loss is connected with electric conduction.

131 H.Javid ave, AZ-1143, Baku
ANAS, G.M.Abdullayev Institute of Physics
E-mail: jophphysics@gmail.com

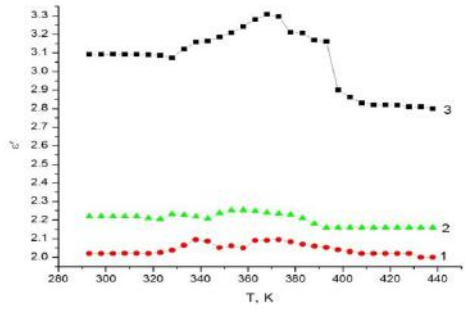

Fig1. The dependence of real part of dielectric constant (ε') in frequency 1kHz on temperature. 1 is pure PP, 2 is PP+2%DK_1, 3 is PP+10%DK_1.

From the dependence on addition volume content at frequency 1 kHz one can see the increase of electric conduction in PP+10%DK_1 composition in comparison with pure PP. From the fig. 2 it is seen the difference of temperature dependences of dielectric losses of pure PP and nano-composites. For pure PP the changes aren't observed and for nano-composites the character of dependence change $tg\delta = f(T)$ differs, i.e. $tg\delta$ increases with temperature increasing. The dependence has the maximum value at temperature of matrix smoothing, further decreasing it passes through minimum near crystallite melting point and it increases again with temperature. In this case, the melting point moves to the side of low-temperature region on 10-15K. Such change of dielectric losses in nano-composites PP+ DK_1 is totally correlated in the dependence on electric conduction on temperature in alternating field.

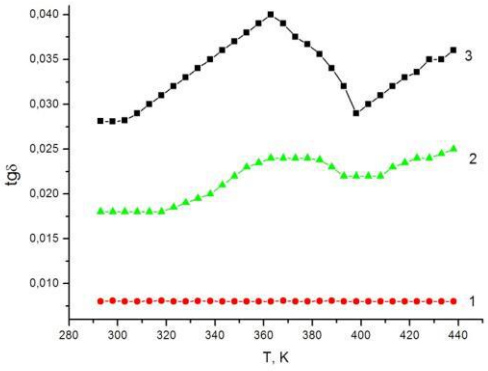

Fig.2. Temperature dependence of tgδ in obtained nano-composites at frequency 1Hz. 1 is pure PP, 2 is PP+2%DK_1, 3 is PP+10%DK_1.

The frequency dependences of ε and tgδ at temperature 20℃ are obtained. From the figures 3 and 4 it is seen that in pure PP and nano-composites at low volume content DK_1 additions aren't revealed with the frequency increase for ε change. ε decreases at big concentrations of addition in obtained nano-composites with frequency increasing. Such characteristic of dielectric loss at low frequencies one can explain by the kinetics of separate structural elements of nano-composite. These structural elements take participation in relaxation processes with frequency increase. As it is mentioned in PP+DK_1 composite the accumulation of DK_1 particles take place in matrix separate parts. These accumulated particles are clusters distribute spontaneously in PP matrix. The cluster number increases with the increase of DK_1 volume content. The clusters closed with each other by sample thickness one can consider as active resistance. As DK_1 has the high conduction with the comparison with PP one so one can consider that composite resistance mainly will be defined by contacts between nano-gel particles.

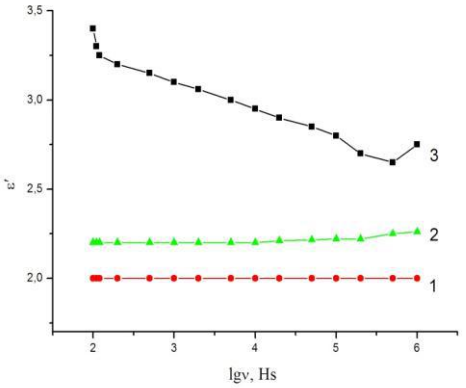

Fig.3. The dependences of (ε') real part on ($lg\nu$) frequency at temperature T=273 K, 1 is pure PP, 2 is PP+2%DK_1, 3 is PP+10%DK_1.

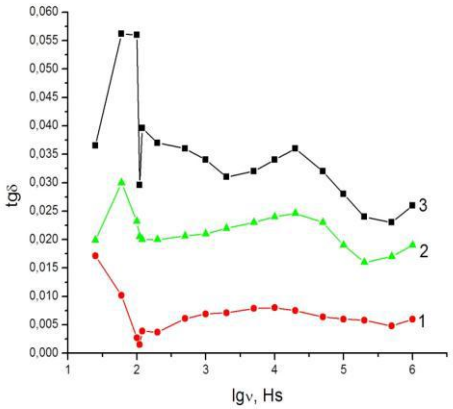

Fig.4. The dependences of dielectric losses at temperature T=293 K on frequency (lgv) 1 is pure PP, 2 is PP+2%DK_1, 3 is PP+10%DK_1.

The accumulation and redistribution of free electric charges (Maxwell-Wagner volume polarization) take place on boundaries of clusters in alternating field. By this fact one can explain the decrease of dielectric strength on DK_1 volume content. Such volume polarization distorts the initial internal electric field at absence of external electric field. It is known that at low frequencies the internal electric field distributes to conduction correspondingly at low frequencies and to dielectric conductions at high frequencies correspondingly.

Consequently, ε decrease with frequency increase can be explained by the appearance of comparably strong internal field in nano-gel –clusters. $tg\delta$ dependence on frequency shows that for pure PP and for PP+2%DK$_1$ nano-composite the maximums at ν=1.5· 10^4 are observed, and also the positive dielectric effect at ν=10^2-1.5· 10^4 Hz frequency because of $tg\delta$ increase in nano-composites is revealed. The inertia of space charge formation in nano-composite structure is observed with frequency increase and it leads to tgδ decrease. At low frequencies the surface charge follows the field and dielectric losses decrease. The polarization in the field of high frequencies doesn't establish for field half-period and dielectric losses decrease. The maximum observable in average frequency region (ν=1.5· 10^4 Hz) of full scale is defined by relaxation losses. The relaxation losses can take place because of low-molecular compounds which have the mobility different degrees. In this case it is carried out at appearance of CO polarization groups. PP partial oxidation takes place in preparation process. tgδ increase in the dependence on frequency depends on polarization process. It is established that the relaxation time in the investigated films at frequencies of less than ones of $\omega=2\pi/T$ variable signal is bigger than Maxwell dielectric relaxation ($\tau_м = \varepsilon\,\varepsilon_o\rho$ where ρ is sample specific resistance in Om·m) and at high frequencies is less than $\tau_м$. The external action time is approximately 100μsec for our films at frequency ν=1.5· 10^4 Hz. The least Maxwell relaxation time is 200msec, i.e. satisfies the condition $\tau < \tau_м$. $tg\delta$ increasing in PP+10%DK$_1$ nano-composite in $\nu \leq 2 \cdot 10^3$ Hz regions shows that dielectric loss in given composites takes place because of electric conduction.

CONCLUSION

Taking into consideration the above mentioned one can propose that polymer stabilizing in the volume, leads to appearance of polar groups on the matrix-nanoparticle boundary. The frequency and temperature dependences in PP polymer and PP+ DK$_1$ and their dielectric properties show that relaxation losses take place because of composite structural elements with mobility different degree and appearance of low-molecular impurities, for example, with appearance of CO polar groups.

[1] *L. Chazeau, J. Cavaille, G. Canova et al.* J. Appl. Polym. Sci., 1999, №71, p. 1797-1808.

[2] *Yu.A. Fedetov, N.N. Smirnova.* Plasticheskie massi, 2008, №9, c. 42-43. (In Russian).

Received:06.09.2016

THE INFLUENCE OF PHOTOVOLTAIC AND PHOTORESISTIVE EFFECTS ON THE FORMATION OF THE PHOTOELECTRET EFFECT IN CdS AND ZnS POLYMER COMPOSITES

G.Z. SULEYMANOV[1], A.F. GOCHUYEVA[2], M.A. KURBANOV[2], F.S. IBRAHIMOVA[1], O.A. ALIYEV[2], S.Ch. ALIYEVA[3]

Institute of Catalysis and Inorganic Chemistry of ANAS[1],
Institute of Physics of ANAS[2],
MES SEDA Hidrotex MMC[3]

It was shown that like in orqanic and inorqanic photosensitive materials photoelectric properties (photoconductivity, photovoltaic, photogeneration and stabilization of electricity charge carries) of the polymer – CdS and polymer – ZnS composities are of great importance as the decisive factor in forming of photoelectret effect.

Keywords: photoelectret, photovoltaic, photorezistivity, photosensitive semiconductor.
PACS: 82,35.Np, 78,67.Bf, 78.55.Et

INTRODUCTION

The mechanism of photoelectret state formation in the polymer composites with photosensitive phase was widely studied in the recent years [1, 3]. It is known, that it is necessary to have two types of relaxers (homo and hetero) for the formation of both electrets and photoelectret effects in any solid material. The electrons injected into composite during photopolarization process and electric charge carrier generated as a result of internal photoeffect belong to the first type of relaxers. There are different kinds of the second relaxer types, including:

- low molecular positive and negative ions having electric load in the polymer matrix;
- colloidal fractions having electric load in the polymer matrix;
- compounds having certain dipole moment in inorganic (CdS, ZnS) and organic (polymer groups, domains, conjugant combination) phases.

The formation of photoelectret effect is possible in the polymer CdS (ZnS) systems having this kind of structure. Certain requirements are set before photoelectrets to meet the growing demand of technique, including electronics. For example, the photoelectrets with different relaxation period are required for photolithography system development. In general, considering photoelectret, photoresistive and photovoltaic effects in materials, for the formation of the above mentioned effects the following common factor comes to the fore:

- creation of charged particles in photopolyarization process and their isolation from one another.

The main goal of our work is to study and define the mechanism of photoelectrete effect formation in polymer - CdS (ZnS) heterogeneous systems. Taking into consideration this goal, the parallel investigation of the mentioned three photoelectret effects in the studied composites is of great importance [1, 3-5].

MATERIALS AND METHODS

The initial phase of the technology of composite obtaining includes: the obtaining of press – crumbs of the components, separating of fractions according to their sizes, blow out from the magnetic separators, cleaning the surface of particles and thermal treatment [6]. The constituents of photocomposities are chosen according to the requirements for them. Thermoplastic polymers such as polyolefine and fluorine-containing polymers were used as polymer phase. CdS, ZnS were used as semiconductor light-sensitive phase.

The working principle of the installations and the blocking scheme used to study photoresistive and photovoltaic effects in polymer-based composites is presented in the work [2]. Generally, photosensitivity is characterized by the ratio of photo current to the dark current. The device used in the study of photoelectret, photovoltaic and photoresistive effects in the composites are extensively considered in the works [1-3, 5, 6] .

The intensity of the light falling on the sample varied between 100 - 600 mWt/sm^2 [2].

RESULTS AND THEIR DISCUSSION

In accordance with the main goal of this work, in order to reveal the formation mechanism of photoelectret effect the main factor in our research was the use and compare of the dependence of composites photoelectrical properties on the share volume of photosensitive phase like all the available composites. Fig. 1, a presents the $I_{ph}/ I_d = f(\Phi)$ dependence for F42 – ZnS and F42 – CdS composities. The experimental results show that the maximum photosensitive semiconductor observed in $I_{ph}/ I_d = f(\Phi)$ dependences are very dependent on phases: if the maximum share is 30% of phase volume for ZnS semiconductor phase composites, the same result for the CdS phase composite is equal to 40%. In the fist approach, this interesting effect should be explained by the interactions with different features occurring in interphase. It should be noted that the maximum observed in $I_{ph}/ I_d = f(\Phi)$ dependence is defferent for F42 - CdS and F42 - ZnS composites. In the first approach, it can be assumed that in the F42 - ZnS compositie the value of the potential interphase barrier is small. This factor is also confirmend by the value of I_{ph}/ I_d ratio.

131 H.Javid ave, AZ-1143, Baku
ANAS, G.M.Abdullayev Institute of Physics
E-mail: jophphysics@gmail.com

In fig. 1, b the dependence of photo electromotive force of polar and non - polar polymers and CdS, ZnS compositions on lightsensitive semiconductor phase is shown. F42- ZnS is the best composite as photovoltaic element. This experimental result is an important factor for clarifying the mechanism of photelectrete effect formation in our work.

a) in the given composites photovoltaic effect depends on the light-sensitive semiconductor phase;

b) photovoltaic effect depends on the polarity, dielectric permittivity and the specific volume resistance of the polymer matrix.

The analysis of the result of studies on photoelectrete effect allows defining the following regularities:

1) in photoelectrete composites consisting of polymer - lightsensitive (CdS, ZnS) semiconductors the photoelectret potential difference U_{phe} first increases according to the increase of the share volume of CdS and ZnS and then decreases after reaching a maximum, increases share volume increases, that is the dependence of $U_{phe} = f(\Phi)$ is of extreme character. On the other hand, a definite relationship between fig.1,a and fig.2 is observed. So, $I_{ph}/I_d=f(\Phi)$ (photoresistive effect) and $U_{phe}=f(\Phi)$ (photoelectrete effect) is of extreme character.

2) there are some difference between various polymers and the composites having light - sensitive semiconductor phases in terms of maximal values of the dependence of photoelectret potential difference U_{phe} on the light - sensitive semiconductor phase share volume; maximum potential difference of polar polymer matrix photocomposities $U_{phe}=f(\Phi)$ dependences are greater than those of non - polar matrix photocomposities (Fig. 2).

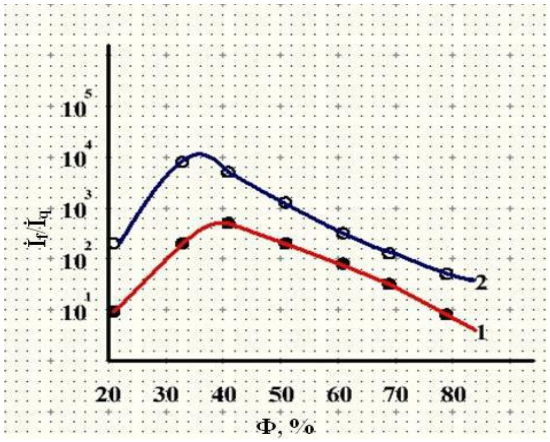

Fig. 1,a. Dependence of F42 – ZnS and F42 – CdS compositions on $I_{ph}/I_d=f(\Phi)$. U=100V,E_l=400 Wt/sm^2.1. F42–CdS; 2. F42–ZnS.

3) the share volume of semiconductor phase corresponding to the maximal value of U_{phe} is smaller for polar polymer matrix composites (Fig. 2).

The extreme character of the obtained dependences caused by the following reasons.

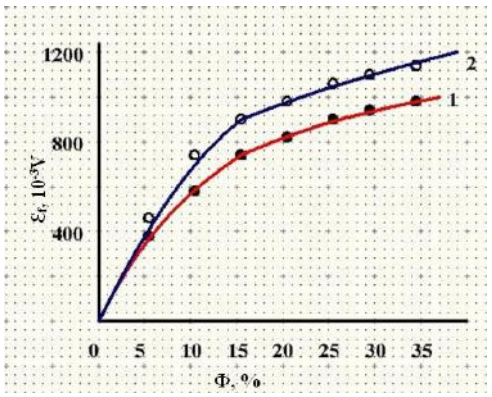

Fig. 1,b. Dependence of photoelectric move force on on the share volume of light- sensitive phase for polar and non- polar polymers, CdS and ZnS based composities. 1.F42 – CdS; 2. F42 – ZnS. Diameter of particles of the semiconductor phase is 6 microns and the sample thickness is 15 microns.

First, oxidation of the polymer matrix and creation of the polar groups forming photoelectrical charge during mechanical mixing of the components under combined effect of temperature and pressure (mechanical termodestruction and termooxidation). Second, change of quasineutral systems forming probability created by homocharges and heterocharges stabilized in interphase border during photoinjection and reduction of $\Delta Q_e=Q_r-Q_{het}$ electrete charge or electrete potential difference defined as homo - and heterocharge superposition. Third, the rise of the composites specific photoconductivity according to the increase of light sensitive phase share volume and the increase of homoelectrical charge relaxation. Fourth, when the share volumes of CdS and ZnS in composite increases, the mass of the polymer phase playing a key role in the electrets formation. Indeed, as a result of the interaction (polymer - light-sensitive CdS and ZnS) between phases, both polymers crystalline structure and CdS and ZnS electronic structure change in the studied composites phase and these effects increase when the share volume of light-sensitive phase rises.

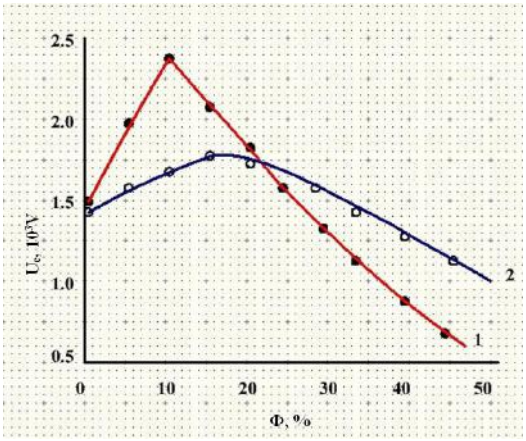

Fig. 2. Dependence of the composites photoelectrete potential difference (Ue) on light-sensitive phase share volume. 1.F42 – ZnS; 2.F42 – CdS. $E_p=0,4\cdot10^4$ V/m; t_p=0,25 hour; E_l=400 mWt/cm^2; T_p=393K..

Thus, in the first approach it can be considered that, the photoelectron prosseses occurring in the interphase boundary play more important role in forming of an photoeletret effect in the composites consisting of polymer photosensitive inorqanic semiconductor materials. We think, that the formation of a new polymer on its nature phase under the influence of polymer – $A^{II}B^{VI}$ photosensitive semiconductor phase are the photoelectret effects. Firs of all, this approach determines the connection between the electret effect and the effects of photoconductivity, photovoltaic and electrical photoquenching. It is known, that free charge carriers, which determine the conductivity owing to internal photoeffect, are forming under the light effect. At the same time, the holes are forming. Now, a possible mechanism of the formation of homo and hetero charges from the abovementioned charges should be clarified. A similar approach should be used for photovoltaic effect. So, the formation of free electrons and holes under the light effect and their subsequent isolation from each other is an essential condition for photoelectret effect forming in the high heterogenic polymer – various inorganic photosensitive phase materials. Electrons are stabilized in traps as deep as possible and certain potential difference is formed during the isolation process. It was determined experimentally that there is no direct connection among photorezistive, photovoltaic and photoelectret effects. So that, the maximums observed in the dependence of I_f/I_q, ε, U_e parameters on the volume share of the composite's photosensitive phase don't fall with each other.

CONCLUSION

The main reason of photoelectret effect formation under the action of light and electricity in the composites based on polymer and CdS, ZnS components is the establishment of homo and hetero charges, which determine the electrets potential difference in electrophotopolyarization proses interphase in the border of composites.

Based on the results of the studies it is concluded, that the major reason of polymer - CdS and polymer - ZnS composites extreme character of $I_{ph}/I_d = f(\Phi)$ and $U_{phe} = f(\Phi)$ dependence is explained with the change of the potential barrier formed in the switch polymer layer between the particles of light-sensitive phase according to the increase of their share volume.

[1] *M.K. Kerimov, M.A. Kurbanov, I.N. Orudjov, A.F. Gochuyeva.* Photoelectret effect in polymer – CdS composite // Reports NASA, 2007, t. LXIII, №3, c. 33 – 37.

[2] *A.F. Gochuyeva.* Photoelectret effect and photo-quenching of the electrical conductivity in the polymer–$A^{II}B^{VI}$ and polymer–ferrocene composites: Ph.D...dis. Baku, 2014, 197 p.

[3] *M.K. Kerimov, M.A. Kurbanov, N.A. Safarov, A.F. Gochuyeva, I.N. Orudjov.* Photoelectret effects of composities on the bases of orqanic and inorqanic polymers and semiconductors. Reports NASA, 2009, t. LXV, №5, p. 33 – 39.

[4] *A.F. Gochuyeva.* Photoelectret effect in composites of F42 sopolymer and CdS / Thezyses of national conference of Physics, mathematics and technical sciences, Nakhchivan, 2008, p.73.

[5] *M. Kerimov, M. Kurbanov, A. Bayramov, N. Safarov, A. Gochuyeva.* New technologies of matrix composite polymer photovoltaic and photoresistive materials. J. Scientific Israel – Technological Advantages, Materials and envoronmental engineering, 2012, v.14, No 4, p. 9 – 15.

[6] *V.P. Mironyuk, Q.V. Kovaleva, T.V. Qriqoreva.* Composite materials in new perspective – elastomers of olefin thermoplastic. L:, Knowledge, 1998, 25 p.

Recevied: 07.10.2016

TRANSPORT PROPERTIES OF $(AgSbSe_2)_{0.9}(PbTe)_{0.1}$

S.S. RAGIMOV, A.A. SADDINOVA
Institute of Physics of Azerbaijan National Academy of Sciences
H.Javid ave., 131, AZ-1143, Baku, Azerbaijan
e-mail: sadiyar@mail.ru

It was investigated the temperature dependence of specific resistivity of $(AgSbSe_2)_{0.9}(PbTe)_{0.1}$ in 40-300K temperature region. A transition to a state with zero resistance similar to the superconducting transition was observed at 66K. The thermal power and Hall- effect were measured in 100-400K temperature interval. It was estimated the carrier concentration and its mobility.

Keywords: thermoelectric material, specific resistivity, thermal power, superconductor phase transition, concentration, temperature dependence.
PACS: 72.20.Pa, 74.25.F

INTRODUCTION

Thermoelectric materials have many applications in the conversion of thermal energy to electrical one. The energy conversion efficiency of a material is characterizes by the thermoelectric figure of merit, $zT = \alpha^2\sigma T/\kappa$. Where α is the Seebeck coefficient (thermal power), σ -electrical conductivity, and κ- thermal conductivity of materials. For improve this efficiency parameter the material by high Seebeck coefficient, high electrical conductivity and low thermal conductivity is required [1-3].

It is known, that the ternary compound $AgSbSe_2$ and PbTe are the thermoelectric material for midrange temperature (400–800 K) applications [1]. $AgSbSe_2$ crystallizes in the NaCl structure where the Ag and Sb atoms are randomly distributed in the Na sites [4]. On the other hand PbTe is also crystallized in the NaCl crystal structure with Pb atoms occupying the cation sites and Te forming the anionic lattice. $AgSbSe_2$ as the other ternary compound of $A^IB^VC_2^{VI}$ system have low thermal conductivity [5]. But the value of electrical conductivity is low at room temperature. To increase the value of electrical conductivity and thermoelectric figure of merit of $AgSbSe_2$ there was sintered the solid solution $(AgSbTe_2)_{0.9}(PbTe)_{0.1}$. The results of experimental investigation of structural and transport properties of $(AgSbSe_2)_{0.9}(PbTe)_{0.1}$ are presented in this work.

EXPERIMENTAL RESULTS AND DISCUSSION

$(AgSbSe_2)_X$ $(PbTe)_{1-X}$ solid solutions material was prepared by direct fusion of stoichiometric amounts of their consistent elements (Ag, Sb, Se, Pb and Te) of purity 99.99% in sealed, evacuated silica ampoule. The ampoule was heated at 1050K for 16 hours with vibrational shaking to ensure homogeneity of the sample. After the synthesis the ampoule was slowly cooled to room temperature.

The phase purity of the obtained sample was investigated by X-ray diffraction and presented in fig.1. The XRD analysis was performed using a Brucker-D8 advance diffractometer at room temperature with scanning mode with a step size $\Delta(2\theta)=0.021^0$ and $5^0 \leq 2\theta \leq 80^0$. From the XRD data, various structural characteristics such as, lattice parameter: (a=b=c=5.8322A, system-cubic, space group (Fm-3m), and grain sizes (813.6A) were deduced.

The resistivity and thermal power were determined by the four-point probe technique. Measurements were taken from a sample in the form of a 8x3x1,2mm parallelepiped. The thermal power was measured by applying a longitudinal heat flux with a constant power released in the heater. A heater was fixed to the end face of the sample by indium. In the range 80-350K, the temperature was measured with copper-constantan thermo-couples. The thermocouples were fixed to the end face of the sample by indium at a distance of 5-6mm. To eliminate the background e.m.f, which is due to a temperature drop between the cold and hot junctions, copper-constantan wires were wound on a copper rod (being in contact with a coolant) immediately at the exit from a cell in which the sample was placed and fixed with BF-2 adhesive. The temperature gradient in the sample between probes varied from 0.5 to 3K.

At room temperature the $(AgSbSe_2)_{0.9}(PbTe)_{0.1}$ exhibit very high thermopower values of about 770 μV/K. The sign of Seebeck coefficient is positive which indicated to hole conductivity and its value decrease slightly with temperature increase.

More interesting results was obtained on the temperature dependence of specific resistivity. The obtained results are presented on fiq.2

The temperature dependence of specific resistivity was measured for two times. At first by the HL5500 PC Hall effect measurement system in the 100-400K temperature interval. The carrier concentration of sample according Hall measurement was $5.9.10^{17}cm^{-3}$ at room temperature. It was estimated the mobility of carriers. The value of mobility was very little $\mu=0.3cm^2/V.s$. At 110K there was observed a maximum on the temperature dependence of electrical resistivity. In order to determine more accurately this situation the measurement was carry out in 40-280K interval of temperature. The value of resistivity at maximum (110K) and room temperature on the temperature dependence were 234kOhm and 97 Ohm respectively. It should be noted that below 110K the value of specific resistivity decrease up to zero at 66K. There is a reasonable question: maybe this is the superconducting transition!? It is known that the superconducting transition T_c plays an important role. Usually the superconducting transition temperature is determined by

131 H.Javid ave, AZ-1143, Baku
ANAS, G.M.Abdullayev Institute of Physics
E-mail: jophphysics@gmail.com

follow way [6]: a) $T_c=T_c(0)$, when the resistivity equal 0; b) T_c equal midpoint of the transition; and c) T_c= T (temperature in the transition region where dρ/dT have a maximum value). The values of T_c estimated by the above-mentioned three methods were 66K, 88K and 93.8K respectively. As seen the temperature range in which the resistivity decreases its zero rather wide (ΔT=44K). It should be noted that all Y-and Bi-based high-temperature superconductors are superconductors of the second kind. The transition temperature interval to the superconducting state is quite wide in these compounds. The temperature dependence of resistivity of high T_c superconductors is mainly metallic in the normal state. On the other hand, in some samples the temperature dependence of the resistivity has a semiconductor behavior in the normal state [7].

According to our knowledge, no studies have been published on the structure and thermoelectric properties of $(AgSbSe_2)_X$ $(PbTe)_{1-X}$ solid solutions. Moreover there is very few studies have been devoted $AgSbSe_2$ at low temperatures [8].

Previously, the temperature dependence of the resistivity of other ternary compounds $A^IB^VC_2^{VI}$ not observed a similar dependence. It seems to us that in any case the observed experimental fact is of great interest. Transition into a state with zero resistance is difficult to explain in this case, excluding superconductivity.

CONCLUSIONS

On the temperature dependence of the specific resistivity of $(AgSbSe_2)_X$ $(PbTe)_{1-X}$ was observed transition into a state with zero resistance at 66K-like superconducting transition.

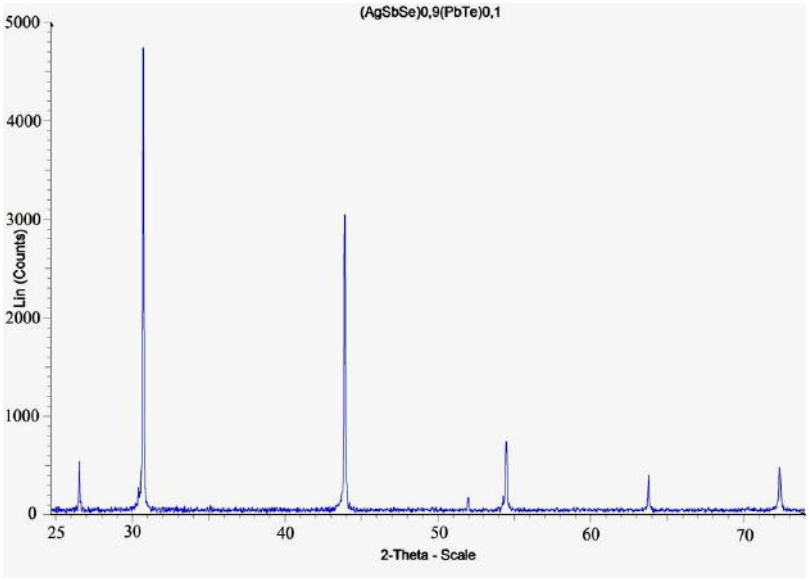

Fig.1. The XRD analysis results of $(AgSbSe_2)_{0.9}(PbTe)_{0.1}$

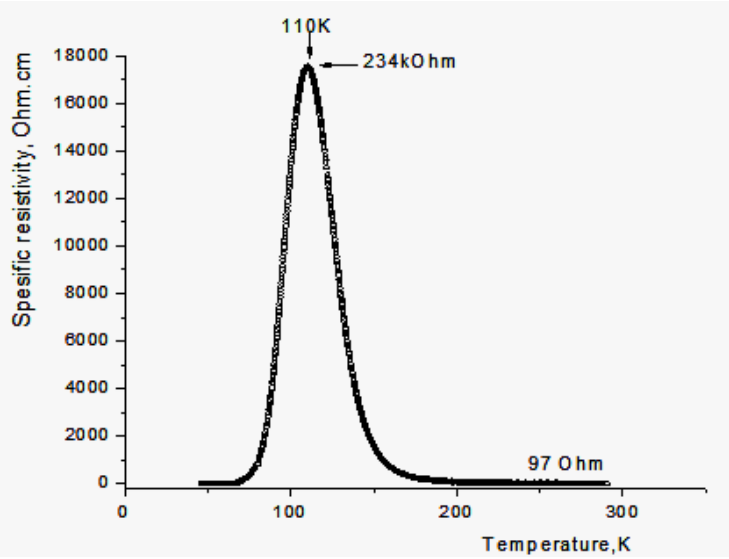

Fiq.2. The temperature dependence of specific resistivity of $(AgSbSe_2)_{0.9}(PbTe)_{0.1}$

[1] *A.V. Dmitriev, I.P. Zavyagin*, Modern trends in the physics of thermoelectric materials, UFN, 2010, v. 180, №8, 821-838. (in Russian)

[2] *K. Wojciechowski, M. Schimidt, J. Tobola, M. Koza, A. Olech, and R. Zybala*. Influence of Doping on Structural and Thermoelectric Properties of $AgSbSe_2$. Journal of Electronic Materials, 2010, v. 39, № 9, p. 2053-2058.

[3] *S.S. Ragimov, S.A. Aliyev, Character* $\alpha \rightarrow \beta$ junction Ag_2Te in the alloy system Ag-Sb-Te, corresponds to the composition $AgSbTe_2$, " Inorganic Materials ", 2007, v.43, p. 1321-1323. (in Russian)

[4] *S. Geller, J.H. Wernick*, Ternary semiconducting compounds witch sodium chloride-like structure: $AgSbSe_2$, $AgSbTe_2$, $AgBiS_2$, $AgBiSe_2$, Acta Cryst. 1959, v. 12, p. 46-52.

[5] *L.D. Dudkin, A.N. Ostranitsa*, Ternary compound semiconductors $A^IB^VC_2^{VI}$, Reports of the USSR Academy of Sciences, 1959, v.124, №1, p. 94-97.

[6] *A.Gauzzi and D.Pavuna*, Evidence for nonuniversal behavior of paraconductivity caused by predominant short-wavelength Gaussian fluctuations in $YBa_2Cu_3O_{6,9}$, Phys. Rew. B, 1995, v.51, N21, p.15420-15428.

[7] *S.A.Kazmin, V.I.Kaydanov, G.Leysing*, Thermal power and resistivity $YBa_2Cu_3O_{7-x}$ oxides, Solid State Physics, 1988, v.30, N10, p.2955-2958. (in Russian)

[8] *T. Namitha Asokan, K.S. Urmila, Rajani Jacob, Rachel Reena Philip, G.S. Okram, V. Ganesa, and B. Pradeep* Optical and electrical properties and phonon drag effect in low temperature TEP measurements of $AgSbSe_2$ thin films. Journal of Semiconductors, 2014, v.35, №.5, p. 052001-1-052001-6.

Received: 03.10.2016

REEXAMINATION A TIME-DEPENDENT HARMONIC OSCILLATOR

Sh.M. NAGIYEV
Institute of Physics, Azerbaijan National Academy of Sciences,
Javid av.131, 1143 Baku, Azerbaijan
E-mail: smnagiyev@physics.ab.az

The evolution operator method has been developed for the study of the time-dependent harmonic oscillator. The invariants and various class of states for the system under consideration are constructed by this method.

Keywords: Time-dependent harmonic oscillator, evolution operator, invariants, exact states.
PACS: 03.65.-w, 03.65.Ge, 03.65.Fd.

1. INTRODUCTION

It is well known that the time-dependent systems for which exact quantum mechanical solutions for the Schrödinger equation can be found are few in number. Both time-dependent harmonic oscillator [1-9] and the time-dependent linear potential [10-14] may be cited as examples. There have been different methods for finding the exact states of the time-dependent systems, such as Lewis-Riesenfeld (LR) invariant method [2], path integral method of Feynman [15], ordinary space-time transformations method [1,9,13] , evolution operator method [16] etc.

The most widely studied time-dependent system is the one-dimensional harmonic oscillator with time-dependent masses or both simultaneously. Besides the intrinsic mathematical interest, the time-dependent harmonic oscillator has many applications in various areas of physics, for example, in quantum optics, plasma physics, molecular physics and quantum chemistry. The harmonic oscillator undoubtedly plays a fundamental role in science.

First the problem of a one-dimensional quantum oscillator with time- dependent frequency moving under the action of a time-dependent force was exactly solved by Husimi [1], who had constructed for this problem Gaussian-type wave packets.

For the oscillator of constant mass and time-dependent frequency LR have introduced [2] an important quantum mechanical invariant I(t) and found the exact quantum states in terms of the invariant eigenstates. Recall that for a system describing by a time-dependent Schrödinger equation

$$\hat{S}(t)\Psi(t) = 0, \qquad \hat{S}(t) = i\hbar\,\partial_t - H(t) \quad (1.1)$$

a Hermitian or non-Hermitian operator $I(t)$ is called an invariant if it commutes with the Schrödinger operator $\hat{S}(t)$, i.e.[$\hat{S}(t), I(t)] = 0$, or, equivalently, satisfies the equation $i\hbar\,\partial_t I(t) + [I(t), H(t)] = 0$. Lewis and Riesenfeld showed [2] that a solution $\Psi_\lambda(t)$ of the time-dependent Schrödinger equation (1.1) and an eigenfunction $\varphi_\lambda(t)$ of $I(t)$ corresponding to an eigenvalue λ ($I(t)\varphi_\lambda(t) = \lambda\varphi_\lambda(t)$ are connected by the relation

$$\Psi_\lambda(t) = e^{i\alpha_\lambda(t)}\varphi_\lambda(t), \quad (1.2)$$

where the time-dependent phase $\alpha_\lambda(t)$ is determined from the Schrödinger equation for $\Psi_\lambda(t)$.

Later the LR invariant method has been generalized to include time-dependent mass and driving force. As a result, exact wave functions have been obtained for harmonic oscillators with time-dependent frequency [3, 4], time-dependent mass and frequency [5-7] and driving force [17]. Two unitary relations between the systems of time-dependent harmonic oscillators were considered in Ref. [8]. The first relation is between the systems of time-dependent mass and of unit mass. The second relation is between those of the driven oscillator and undriven (see, also, [1]). Ciftja [9] found a solution of the harmonic oscillator with time-dependent mass and frequency by employing some simple space-time transformations.

The purpose of the present paper is to study the general problem of the harmonic oscillator with time-dependent mass and frequency moving under the action of a time-dependent force by using an evolution operator method. As is well known this method has been long time used to solve the problems in quantum mechanics and quantum field theory. In our study we have found that the evolution operator method is much simpler for deriving the quantum-mechanical quantities than other methods.

The evolution operator U(t) obeys Schrödinger equation (1.1) $\hat{S}(t)U(t) = 0$ with the obvious initial condition U(0)=1. According to the principles of quantum mechanics all the information on the dynamics of quantum system is contained in the matrix elements of the evolution operator.

$$U(t) = T\exp\left(-\frac{i}{\hbar}\int_0^t H(t')dt'\right). \quad (1.3)$$

The evolution operator of the wave function $\Psi(t)$ (the solution of the Schrödinger equation (1.1)) is determined by the evolution operator, i.e.

$$\Psi(t) = U(t)\Psi(0), \quad (1.4)$$

where $\Psi(0)$ is initial wave function.

From the general representation (1.4) for the solutions of the Schrödinger equation (1.1) .It is evident

131 H.Javid ave, AZ-1143, Baku
ANAS, G.M.Abdullayev Institute of Physics
E-mail: jophphysics@gmail.com

that this equation has infinitely many solutions. Using different initial wave functions $\Psi(0)$, one can construct different wave functions $\Psi(t)$ at any later time $t > 0$

An evolution operator allows us also to construct the LR invariants for a given quantum system. The point is that any invariant for a quantum system can be expressed in terms of (through) two linearly independent simple invariants, such as $\hat{p}_0(t)$ and $\hat{x}_0(t)$ which are the initial momentum and coordinate operators, respectevly:

$$\hat{p}_0(t) = U(t)\hat{p}U^{-1}(t), \quad \hat{x}_o(t) = U(t)\hat{x}U^{-1}(t). \quad (1.5)$$

Therefore, any invariant $I(t)$ can be represented in the form $I(t) = U(t)I(0)U^{-1}(t)$, where $I(0) = G(\hat{p}, \hat{x})$ is any function of $\hat{p}$ and $\hat{x}$.

2. THE EVOLUTION OPERATOR

The Schrödinger equation for the harmonic oscillator with time-dependent mass $M(t)$ and frequency $\omega(t)$under the force $F(t)$ is

$$i\hbar\partial_t\Psi(t) = H(t)\Psi(t) \quad (2.1a)$$

with the time-dependent Hamiltonian

$$H(t) = -\frac{\hbar^2}{2M(t)}\partial_x^2 + \frac{1}{2}M(t)\omega^2(t)x^2 - F(t). \quad (2.1b)$$

It is convenient at first to reduce the problem (2.1) to the simpler case of vanishing $F(t)$. For this aim we perform an unitary transformation (compare with [1])

$$\Psi(x,t) = U_1(t)\Psi_1(x,t) \quad (2.2)$$

with the unitary operator

$$U_1(t) = \exp[-\xi(t)\partial_x]\exp\{\frac{i}{\hbar}\left[M(t)\dot{\xi}(t)x + \sigma(t)\right]\}, \quad (2.3)$$

where $\xi(t)$ satisfies the classical equation of motion

$$\frac{d}{dt}\left[M(t)\dot{\xi}(t)\right] + M(t)\omega^2(t)\xi(t) = F(t) \quad (2.4)$$

and $\sigma(t)$ is the classical action for the harmonic oscillator

$$\sigma(t) = \int_0^t [\frac{1}{2}M(t')\dot{\xi}^2(t') - \frac{1}{2}M(t')\omega^2(t')\xi^2(t') + F(t')\xi(t')dt'. \quad (2.5)$$

Note that $\xi(t)$ may, without loss of generality, be assumed to be that solution of equation (2.4), which initially vanishes together with its derivative $\dot{\xi}(t)$ [1], i.e.

$$\xi(0) = 0, \dot{\xi}(0) = 0. \quad (2.6)$$

From this it is evident that, the initial condition $U_1(0) = 1$ for $U_1(t)$ is holds. Moreover, it is clear that if $F(t) \equiv 0$, than $\xi(t) \equiv 0$.

As result if this fact the eq. (2.1a) has the following form:

$$i\hbar\partial_t\Psi_1(x,t) = H_1(t)\Psi_1(x,t), \quad (2.7a)$$

where

$$H_1(t) = -\frac{\hbar^2}{2M(t)}\partial_x^2 + \frac{1}{2}M(t)\omega^2(t)x^2. \quad (2.7b)$$

The wave function satisfies the initial condition $\Psi_1(x,0) = \Psi(x,0)$.
In the next step we take the wave function $\Psi_1(x,t)$ in the form

$$\Psi_1(x,t) = U_2(t)\Psi_2(x,t), \; U_2(t) = e^{i\alpha(t)x^2}, \quad (2.8)$$

where the time-dependent real function $\alpha(t)$ with the initial condition $\alpha(0) = 0$ is to be found later.

Substituting equation (2.8) into (2.7a) we obtain

$$i\hbar\partial_t\Psi_2(x,t) = \{-\frac{\hbar^2}{2M(t)}\partial_x^2 + [\hbar\,\dot{\alpha}(t) + \frac{2\hbar^2}{M(t)}\alpha^2(t) + \frac{1}{2}M(t)\omega^2(t)]x^2 - \frac{i\hbar^2}{M(t)}\alpha(t)(\partial_x x + x\partial_x)\}\Psi_2(x,t) \quad (2.9)$$

To simplify this equation we choose the auxiliary time-dependent function $\alpha(t)$ in such a way that the coefficient of x^2 vanishes. As a result we easily find that $\alpha(t)$ must satisfy the first-order nonlinear differential equation (Riccati equation)

$$\dot{\alpha}(t) + \frac{2\hbar}{M(t)}\alpha^2(t) = -\frac{1}{2\hbar}M(t)\omega^2(t). \tag{2.10}$$

This condition put on the auxiliary time-dependent function $\alpha(t)$ allows us to write equation (2.9) as

$$i\hbar\partial_t\Psi_2(x,t) = H_2(t)\Psi_2(x,t), \tag{2.11}$$

where the time-dependent Hamiltonian $H_2(t)$ is equal to

$$H_2(t) = -\frac{\hbar^2}{2M(t)}\partial_x^2 - \frac{2i\hbar^2}{M(t)}\alpha(t)\partial_x x + \frac{i\hbar^2}{M(t)}\alpha(t). \tag{2.12}$$

Introducing instead of $\alpha(t)$ a new function $\eta(t)$ by the relation

$$\alpha(t) = \frac{M(t)\dot{\eta}(t)}{2\hbar\,\eta(t)} \tag{2.13}$$

we transform the Riccati equation (2.12) to the form of the linear differential equation of the second-order:

$$\frac{d}{dt}[M(t)\dot{\eta}(t)] + M(t)\omega^2(t)\eta(t) = 0\,. \tag{2.14}$$

From the condition $\alpha(0) = 0$ follows that $\eta(0) \neq 0$ and $\dot{\eta}(0) = 0$.
Finally, we want to find the evolution operator $U_3(t)$ for the equation (2.11) with the Hamiltonian (2.12):

$$U_3(t) = T\exp\{-\frac{i}{\hbar}\int_0^t H_2(t')dt'\}\,,\;\; U_3(0) = 1. \tag{2.15}$$

Note that a method to disentangle this type exponential operators into a product of the exponential operators was given in Ref. [18] (see, Appendix). Using this method, one can represent the evolution operator $U_3(t)$ (2.15) as follows:

$$U_3(t) = e^{\frac{1}{2}\delta(t)(\partial_x x + x\partial_x)}e^{iS(t)\partial_x^2}\,, \tag{2.16}$$

where

$$\delta(t) = -2\hbar\int_0^t \frac{\alpha(t')}{M(t')}dt'\,, \qquad S(t) = \hbar\int_0^t \frac{e^{2\delta(t')}}{2M(t')}dt'\,. \tag{2.17}$$

It is clear that the evolution operator $U(t)$ for the equation (2.11) is just the product of the operators $U_1(t)$ (2.3), $U_2(t)$ (2.8) and $U_3(t)$ (2.16), i.e. $U = U_1U_2U_3$, or explicitly

$$U(t) = e^{-\frac{1}{2}\delta(t)+\frac{i}{\hbar}\sigma(t)}e^{-\xi(t)\partial_x}e^{\frac{i}{\hbar}M(t)\dot{\xi}(t)x}e^{i\alpha(t)x^2}e^{\delta(t)\partial_x x}e^{iS(t)\partial_x^2}\,. \tag{2.18}$$

This operator is unitary and satisfies the initial condition $U(0) = 1$. The solution of the Schrödinger equation (2.1) can be written now in the symbolic form

$$\Psi(x,t) = U(t)\Psi(x,0). \tag{2.19}$$

For simplicity in what follows we consider only the case $F(t) \equiv 0$. Then $U(t)$, instead of (2.18), will be givem by

$$U(t)=e^{-\frac{1}{2}\delta(t)}e^{i\alpha(t)x^2}e^{\delta(t)\partial_x x}e^{iS(t)\partial_x^2}. \tag{2.20}$$

As an example, we find an explicit form of the operator (2.20) for the particular case, when $M(t)=m$ and $\omega(t)=\omega_o$. In this case η is the solution of the equation $\ddot{\eta}(t)+\omega_o^2\eta(t)=0$, which must satisfy the conditions $\eta(0)=\eta_0$, $\dot{\eta}(0)=0$. This solution is $\eta=\eta_0\cos\omega_0(t)$. Then we easily obtain from (2.13), (2.16) and (2.17):

$$\alpha(t)=-\frac{m\omega_0}{2\hbar}\tan(\omega_0 t),$$

$$\delta(t)=-\ln(\cos\omega_0 t)\,, \tag{2.21}$$

$$s(t)=\frac{\hbar}{2m\omega_0}\tan(\omega_0 t).$$

Substituting (2.21) into (2.20) one get the following expression for the evolution operator

$$U(t)=e^{-\frac{im\omega_0}{2\hbar}\tan(\omega_0 t)x^2}e^{\frac{i\hbar}{4m\omega_0}\sin(2\omega_0 t)\partial_x^2}e^{-\ln(\cos\omega_o t)(x\partial_x+1/2)}\,, \tag{2.22}$$

which coincides with the well known formula (see, for example, [19]).

As is known, the time dependent Schrödinger equation, describing any quantum system has in finitely many solutions. Having found the evolution operator (2.20) and appropriately choosing the initial wave function in (2.19) one can construct any solution of the equation (2.1). The evolution operator method allows as to construct also LR invariants for the given system by the simple way.

3. INVARIANTS

First of all we find an explicit form of $\hat{p}_0$ and $\hat{x}_0$. Taking into account the explicit form (2.20) of the evolution operator we get

$$\begin{aligned}\hat{p}_0(t)&=a_1(t)\hat{p}-M(t)\dot{a}_1(t)\hat{x}\,,\quad \hat{p}_0(0)=\hat{p}\,,\\ \hat{x}_0(t)&=a_2(t)\hat{p}-M(t)\dot{a}_2(t)\hat{x},\quad \hat{x}_0(0)=\hat{x}\,,\end{aligned} \tag{3.1}$$

where $a_1(t)=\exp[-\delta(t)]$, $a_2(t)=-2S(t)a_1(t)/\hbar$. We now define the time-dependent annihilation and creation operators

$$a(t)=\frac{1}{\sqrt{2}}\left(\lambda\hat{x}_0+\frac{i\hat{p}_0}{\lambda\hbar}\right),\qquad a^+(t)=\frac{1}{\sqrt{2}}\left(\lambda\hat{x}_0-\frac{i\hat{p}_0}{\lambda\hbar}\right), \tag{3.2}$$

where $\lambda=(m\omega_0/\hbar)^{-1/2}$, $m=M(0)$ and $\omega_0=\omega(0)$. Next, let us rewrite the operators (3.2) as

$$a(t)=\frac{i}{\sqrt{2\hbar}}[\varepsilon(t)\hat{p}-M(t)\dot{\varepsilon}(t)x],\qquad a^+(t)=\frac{-i}{\sqrt{2\hbar}}[\varepsilon^*(t)\hat{p}-M(t)\dot{\varepsilon}^*(t)x] \tag{3.3}$$

with the function

$$\varepsilon(t)=(m\omega_0)^{-1/2}[1+2im\omega_0 S(t)/\hbar]a_1(t)\,, \tag{3.4}$$

which satisfies the initial conditions $\varepsilon(0)=(m\omega_0)^{-1/2}$ and $\dot{\varepsilon}(0)=i(\omega_0/m)^{1/2}$. Using (2.10) one can show that the complex function $\varepsilon(t)$ obeys the equation (compare with Ref. [20], where the $M(t)=m$ case was considered)

$$\frac{d}{dt}\left[M(t)\dot{\varepsilon}(t)\right]+M(t)\omega^2(t)\varepsilon(t)=0 \tag{3.5}$$

and the relation $M\left(\dot{\varepsilon}\varepsilon^*-\dot{\varepsilon}^*\varepsilon\right)=2i$.

Let us put $\varepsilon(t)\equiv\rho(t)\exp\left[i\gamma(t)\right]$, where $\rho(t)=|\varepsilon(t)|$ and $\gamma(t)=\int_0^t dt'/M(t')\rho^2(t')$. Then from the equation (3.5) it follows that the function $\rho(t)$ satisfies an equation

$$\ddot{\rho}(t)+\frac{\dot{M}(t)}{M(t)}\dot{\rho}(t)+\omega^2(t)\rho(t)=\frac{1}{M^2(t)\rho^3(t)}\ . \tag{3.6}$$

We can express all quantities in terms of function $\rho(t)$. For example, we have

$$\delta(t)=-\ln(\rho\cos\gamma/\rho_0),$$

$$S(t)=\tan\gamma/2\lambda^2,$$

$$\alpha(t)=\left(\frac{M\dot{\rho}}{\rho}-\frac{\tan\gamma}{\rho^2}\right)/2\hbar,$$

$$\hat{p}_0(t)=\frac{1}{\rho_0}\left[\frac{\hat{x}}{\rho_0}\sin\gamma+\left(\rho\hat{p}-M\dot{\rho}\hat{x}\right)\cos\gamma\right], \tag{3.7a}$$

$$\hat{x}_0(t)=\rho_0\left[\frac{\hat{x}}{\rho}\cos\gamma-\left(\rho\hat{p}-M\dot{\rho}\hat{x}\right)\sin\gamma\right], \tag{3.7b}$$

$$a(t)=\frac{1}{\sqrt{2\hbar}}\left[\frac{\hat{x}}{\rho}+i\left(\rho\hat{p}-M\dot{\rho}\hat{x}\right)\right]e^{i\gamma},$$

$$a^+(t)=\frac{1}{\sqrt{2\hbar}}\left[\frac{\hat{x}}{\rho}-i\left(\rho\hat{p}-M\dot{\rho}\hat{x}\right)\right]e^{-i\gamma}\ , \tag{3.7c}$$

$$a_1(t)=\rho\cos\gamma/\rho_0,\qquad a_2(t)=-\rho_0\rho\sin\gamma,$$

where $\rho_0\equiv\rho(0)$. In the simple ease, when $M(t)=m,\ \omega(t)=\omega_0$,we have

$$\hat{p}_0=\hat{p}\cos\omega_0(t)+m\omega_0 x\sin\omega_0 t,\quad \hat{x}_0(t)=-\frac{\hat{p}}{m\omega_0}\sin\omega_0 t+x\cos\omega_0 t\,.$$

The operators $a(t)$ and $a^+(t)$, in deference of operators a и a^+ in [6], are the linear invariants. From them we construct the quadratic invariant

$$I_2(t)=a^+(t)a(t)+\hbar/2=\frac{1}{2}\left[\frac{x^2}{\rho^2}+\left(\rho\hat{p}-M\dot{\rho}x\right)^2\right]. \tag{3.8}$$

This formula is a generalization LR invariant [2] to the case of time-dependent mass [7] [21].

4. WAVE FUNCTIONS

From the general (symbolic) representation

$$\Psi(x,t)=e^{\frac{1}{2}\delta(t)}e^{i\alpha(t)x^2}e^{\delta(t)x\partial_x}e^{iS(t)\partial_x^2}\Psi(x,0) \tag{4.1}$$

for the solutions of the time-dependent Schrödinger equation (2.1) ($F(t)\equiv 0$) we can construct infinitely many wave functions. We will consider there type wave functions:

1) Plane wave type initial wave function

$$\Psi(x,t)=\frac{1}{\sqrt{2\pi\hbar}}\exp\left(ip_0x/\hbar\right). \tag{4.2}$$

Using the formula (A.3) at $\lambda=0$ we get the wave function

$$\Psi(x,t)=\frac{1}{\sqrt{2\pi\hbar}}\exp\left[\frac{1}{2}\delta(t)+\frac{ip_0x}{\hbar}e^{\delta(t)}+i\alpha(t)x^2-\frac{iS(t)}{\hbar^2}p_0^2\right]. \tag{4.3}$$

We express the wave function (4.3) in terms of $\rho(t)$:

$$\Psi(x,t)=\sqrt{\frac{\rho_0}{2\pi\hbar\rho\cos\gamma}}\exp\left\{\frac{i}{\hbar}\left[\frac{1}{2}\left(\frac{M\dot{\rho}}{\rho}-\frac{\tan\gamma}{\rho^2}\right)x^2-\frac{1}{2}\rho_0^2p_0^2\tan\gamma+\frac{\rho_0p_0x}{\rho\cos\gamma}\right]\right\}. \tag{4.4}$$

In the particular case, when $M(t)=m$, $\omega(t)=\omega_0$ we have

$$\Psi(x,t)=\frac{1}{\sqrt{2\pi\hbar\cos\omega_0t}}\exp\left[-\frac{i}{\hbar}\left(\frac{m\omega_0x^2}{2}+\frac{p_0^2}{2m\omega_0}-\frac{p_0x}{\sin\omega_0t}\right)\tan\omega_0t\right]. \tag{4.5}$$

2). Airy type initial wave function

$$\Psi(x,t)=Ai(Bx). \tag{4.6}$$

With the help of the formula (A.4) we find that in this case the wave function has a form

$$\Psi(x,t)=\exp\left[\frac{1}{2}\delta(t)+i\alpha(t)x^2\right]\exp\left[iS(t)B^3e^{\delta(t)}x-\frac{2}{3}iS^3(t)B^6\right]A\left(Be^{\delta(t)}x-S^2(t)B^4\right) \tag{4.7}$$

or in terms of $\rho(t)$ we have

$$\Psi(x,t)=\sqrt{\frac{\rho_0}{\rho\cos\gamma}}\exp\left\{-\frac{iB^6\tan^3\gamma}{12\lambda^6}+\frac{i\rho_0B^3\tan\gamma}{2\lambda^2\rho\cos\gamma}x+\frac{i}{2\hbar}\left(\frac{M\dot{\rho}}{\rho}-\frac{\tan\gamma}{\rho^2}\right)x^2\right\}\cdot$$
$$\cdot Ai\left(\frac{\rho_0B}{\rho\cos\gamma}x-\frac{B^4\tan^2\gamma}{4\lambda^4}\right) \tag{4.8}$$

If we take in (4.8) $M(t)=m$ and $\omega(t)=\omega_0$, then

$$\Psi(x,t)=\frac{1}{\sqrt{\cos\omega_0 t}}\exp\left\{-\frac{iB^6\tan^3\omega_0 t}{12\lambda^6}+\frac{iB^3\tan\omega_0 t}{2\lambda^2\cos\omega_0 t}x-\frac{\lambda^2\tan\omega_0 t}{2}x^2\right\}\cdot$$

$$\cdot Ai\left(\frac{Bx}{\cos\omega_0 t}-\frac{B^4\tan^2\omega_0 t}{4\lambda^4}\right) \tag{4.9}$$

3) Oscillator type initial wave function:

$$\Psi_n(x,0)=c_n e^{-\frac{\lambda^2x^2}{2}}H_n(\lambda x),\quad c_n=c_0/\sqrt{2^n n!}, \tag{4.10}$$

$$c_0=\left(\lambda^2/\pi\right)^{1/4}.$$

Using now (A.5) in (4.1) one obtains then the wave function corresponding to (4.10)

$$\Psi_n(x,t)=c_n\frac{e^{\frac{1}{2}\delta(t)}}{\sqrt{1+2i\lambda^2S(t)}}\left(\frac{1-2i\lambda^2S(t)}{1+2i\lambda^2S(t)}\right)^{\frac{n}{2}}e^{Ax^2}H_n\left(\frac{\lambda e^{\delta(t)}x}{\sqrt{1+4\lambda^4S^2(t)}}\right), \tag{4.11}$$

where

$$A=i\alpha(t)-\frac{\lambda^2e^{2\delta(t)}}{2\left(1+2i\lambda^2S(t)\right)}.$$

In terms of the function $\rho(t)$ the wave function (4.11) takes the form

$$\Psi_n(x.t)=c_n(\rho_0/\rho)^{\frac{1}{2}}e^{-i\left(n+\frac{1}{2}\right)\gamma}\exp\left[\frac{i}{2\hbar}\left(\frac{M\dot\rho}{\rho}+\frac{i}{\rho^2}\right)x^2\right]H_n\left(\frac{1}{\sqrt{\hbar}}\frac{x}{\rho}\right), \tag{4.12}$$

which agrees with the result of Ref. [7]. The functions (4.12) are the eigenfunctions of the invariant $I_2(t)$ (3.8) with the eigenvalues $\lambda_n=\left(n+\frac{1}{2}\right)\hbar$ and $a(t)\Psi_n(x,t)=\sqrt{n}\Psi_{n-1}(x.t)$, $a^+(t)\Psi_n(x,t)=\sqrt{n+1}\Psi_{n+1}(x,t)$.

In the particular case, when $M(t)=m$ and $\omega(t)=\omega_0$ from (4.12) it follows the well-known result:

$$\Psi_n(x,t)=c_n e^{-i\left(n+\frac{1}{2}\right)\omega_0(t)}e^{-\frac{\lambda^2x^2}{2}}H_n(\lambda x)=e^{-i\left(n+\frac{1}{2}\right)\omega_0 t}\Psi_n(x,0). \tag{4.13}$$

5. CONCLUSION

We have studied Schrödinger equation for a time-dependent harmonic oscillator with the help of the evolution operator method. Our analysis has shown that the key of solving the time-dependent Schrödinger equation is to find an evolution operator $U(t)$ of the system. This is explained by the following facts: 1) In this case, unlike LR invariant method, there is no further problem of finding the time-dependent phase; 2)The general representation for the wave function in terms of the evolution operator $\psi(t)=U(t)\psi(0)$ allows us to get any kinds of solutions of Schrödinger equation and with muchless efforts; 3) The evolution operator allows us to find not only solutions of the time-dependent Schrödinger equation, but also to construct all kinds of invariants.

APPENDIX

1. Note that operators $e^{\delta x\partial_x}$ and $e^{\alpha\partial_x^2}$ acts on functions $f(x)$ in following form:

$$e^{\delta x\partial_x} f(x) = f\left(e^{\delta} x\right), \tag{A.1}$$

$$e^{\alpha\partial_x^2} f(x) = \frac{1}{\sqrt{4\pi\alpha}} \int_{-\infty}^{\infty} e^{-\frac{(x-z)^2}{4\alpha}} f(z)dz = \sum_{-\infty}^{\infty} \frac{\alpha^n}{n!} f^{(2n)}(x). \tag{A.2}$$

Examples:

1) $$e^{\alpha\partial_x^2} e^{-\lambda x^2+\gamma x} = (1+4\alpha\lambda)^{-1/2} \exp\left[-\left(\lambda x^2 - \gamma x - \alpha\gamma^2\right)/(1+4\alpha\lambda)\right], \tag{A.3}$$

2) $$e^{\alpha\partial_x^2} e^{\gamma x} Ai(Bx) = e^{\varphi(x)} Ai\left(Bx + 2\alpha\gamma B + \alpha^2 B^4\right),$$

$$\varphi(x) = \left(\gamma + \alpha B^3\right)x + \alpha\gamma\left(\gamma + 2\alpha B^3\right) + \frac{2}{3}\alpha^3 B^6, \tag{A.4}$$

3) $$e^{\alpha\partial_x^2} e^{-\frac{1}{2}\lambda^2 x^2} H_n(\lambda x) = \left(1+2\alpha\lambda^2\right)^{-1/2} \left(\frac{1-2\alpha\lambda^2}{1+2\alpha\lambda^2}\right)^{n/2} \exp\left[-\frac{\lambda^2 x^2}{2\left(1+2\alpha\lambda^2\right)}\right] H_n\left(\frac{\lambda x}{\sqrt{1-2\alpha^2\lambda^4}}\right), \tag{A.5}$$

where $Ai(x)$ is the Airy function and $H_n(\lambda x)$ is Hermite polynomial. To derive the formula (A.4) we have used the integral [22]

$$\int_{-\infty}^{\infty} e^{-p(x-y)^2} H_n(cx)dx = \sqrt{\frac{\pi}{p}} \left(\frac{p-c^2}{p}\right)^{n/2} H_n\left(cy\sqrt{\frac{p}{p-c^2}}\right), \ y, \ \text{Re}\, p > 0. \tag{A.6}$$

---

[1] *K. Husimi.* Progr. Theor. Phys. 9 (1953) 381.
[2] *H.R. Lewis, W.B. Riesenfeld.* J. Math. Phys.10 (1969) 1458.
[3] *C. M. A. Dantas, I.A. Pedrosa, B. Baseia.* Phys. Rev. A 45 (1992) 1320.
[4] *K.H. Yeon, H.J. Kim, C I. Um, T.F. George, L. N. Pandey.* Phys. Rev. A 50. (1994) 1035
[5] *J.Y. Ji, J.K. Kim, S.P. Kim.* Phys. Rev. A 51 (1995) 4268.
[6] *J.Y. Ji, J.K. Kim, K.S. Soh.* Phys. Rev. A 52 (1995) 3352.
[7] *I.A. Pedrosa.* Phys. Rev A 55 (1997) 3219.
[8] *D.Y. Song.* J. Phys. A: Math. Gen. 32 (1999) 3449.
[9] *O. Ciftja.* J. Phys. A: Math. Gen. 32 (1999) 6385.
[10] *M.V. Berry, N.L. Balazs.* Am. J. Phys. 47 (1979) 264.
[11] *V.V. Dodonov, V.I. Manko, O.V. Shakhnistova.* Phys. Lett. A 102 (1984) 295.
[12] *I. Guedes,* Phys. Rev. A 63 (2001) 034102.
[13] *M. Fend.* Phys. Rev. A 64 (2002) 034101.
[14] *P.G. Luan, C.Sh. Tang.* Phys. Rev. A71 (2005) 014101.
[15] *R.P. Feynman, A.R. Hibbs.* Quantum Mechanics and Path Integrals
[16] (Mc Graw-Hill, New York, 1965).
[17] *F.J. Dyson.* Phys. Rev. 75 (1949) 1736.
[18] *H.C. Kim, M.H. Lee, J.Y. Ji, J.K. Kim.* Phys. Rev. A 53 (1996) 3767.
[19] *Sh. M. Nagiyev.* Azerb. J. Physics (Fizika), 2013, vol. XIX №2, sec:Az, pp.129-135.
[20] *W. Qinmou.* J. Phys. A20 (1987) 5041.
[21] *V.V. Dodonov, I.A. Malkin, V.I. Manko.* Physica 72 (1974) 597.
[22] If a printing error in eq. (4) Ref. [7] is corrected, i. e. replacing $\left(\frac{q}{\rho}\right)^{\frac{1}{2}}$ with $\left(\frac{q}{\rho}\right)^{2}$. We can easily find that eq. (4) of Ref. [7] is identical to eq. (3.8) in the present paper.
[23] *A.P. Prudnikov, Yu.A. Brychkov, O.I. Marichev.* Integrals and Series, vol. 2. Special Functions, Gordon and Breach. New York (1988).

Received: 19.09.2016

THE NEW UNKNOWN FIELD CAUSED BY VARYING IN TIME GRAVITATIONAL FIELD

H.F. ABBASOV
"OilGasScientificResearchProject" Institute, SOCAR
AZ1012, H.Zardabi 88a, Baku, Azerbaijan
abbasovhakim@gmail.com

By using an analogy between the gravitational field and electric field (Coulomb's law and Newton's law of gravity), it has been proposed that the change of gravitational field over time should lead to the emergence of a new vortex field similar vortex magnetic field due to the Maxwell's bias current. The gravitational field and the new vortex field create one another and spread in space, always remaining perpendicular to one another and to the spreading direction, similarly to the electric and magnetic fields in electromagnetic wave. The occurrence of black holes, dark energy and dark matter can be explained by existence of new vortex field.

Key words: new vortex field, gravitational field, electric field, magnetic field.
PACS: 98.80.-k, 95.36.+x

INTRODUCTION

According to the Gauss's law [1] the flux of the gravitational field, created by a single particle of mass m through the closed surface equals to:

$$\int \vec{g} d\vec{S} = 4\pi G m \tag{1}$$

where $\vec{g}$ is the gravitational field, $d\vec{S}$ is the surface element, G is the gravitational constant.
Formula (1) can be rewritten in differential form by using Gauss's theorem as,

$$\int \vec{g}\, d\vec{S} = \int div\vec{g}\, dV = 4\pi G \int \rho dV$$

or

$$div\vec{g} = 4\pi G\rho \tag{2}$$

where ρ is the density of the particle of mass m and of volume V.

BASIC EQUATIONS

By using an analogy between the gravitational field and electric field (Coulomb's law and Newton's law of gravity), we can conclude that the change of $\vec{g}$ over time should lead to the emergence of a new vortex field $\vec{X}$ (similar Maxwell's equation for bias current [2, 3]):

$$\int X_l dl = -\frac{d}{dt}\int \vec{g} d\vec{S} = -4\pi G \frac{dm}{dt} = -4\pi G V \frac{d\rho}{dt} - 4\pi G\rho \frac{dV}{dt} \tag{3}$$

or by using the Stokes's theorem we obtain,

$$rot\vec{X} = -\frac{\partial \vec{g}}{\partial t} \tag{4}$$

Besides, the change of $\vec{X}$ over time should lead to the emergence of a new vortex gravitational field $\vec{g}$ (similarly, Faraday's law of induction [4]):

$$\int g_l dl = -\frac{1}{v^2}\frac{d}{dt}\int \vec{X} d\vec{S} \tag{5}$$

where v is some parameter.
By using the Stokes' theorem formula (5) can be rewritten in differential form as,

$$rot\vec{g} = -\frac{1}{v^2}\frac{\partial \vec{X}}{\partial t} \tag{6}$$

Producing operation rot in both parts of equation (6) and substituting the expression of $rot\vec{X}$ from equation (4) we obtain:

$$rotrot\vec{g} = -\frac{1}{v^2}\frac{\partial}{\partial t} rot\vec{X} \tag{7}$$

or

$$rotrot\vec{g} = -\frac{1}{v^2}\frac{\partial^2 \vec{g}}{\partial t^2} \tag{8}$$

It is the wave equation for gravitational field, that spreads in space with the speed v. In case $\vec{g}(0,0,g_z)$ and $g_z(x)$ after some simplifications we obtain

$$\frac{\partial^2 g_z}{\partial x^2} = \frac{1}{v^2}\frac{\partial^2 g_z}{\partial t^2} \tag{9}$$

that we can solve as,

$$g_z = g_{z0} e^{i(\omega t - kx)} \tag{10}$$

Actually, by substituting this function to the (9) we obtain the wave vector:

$$k = \frac{\omega}{v} = \frac{2\pi\nu}{v} = \frac{2\pi}{\lambda} \tag{11}$$

Analogically, producing operation rot in both parts of equation (4) and substituting the expression of $rot\vec{g}$ from equation (6) we obtain:

131 H.Javid ave, AZ-1143, Baku
ANAS, G.M.Abdullayev Institute of Physics
E-mail: jophphysics@gmail.com

$$rotrot\vec{X} = -\frac{1}{v^2}\frac{\partial}{\partial t}rot\vec{g} \quad (12)$$

or

$$rotrot\vec{X} = -\frac{1}{v^2}\frac{\partial^2\vec{X}}{\partial t^2} \quad (13)$$

It is the wave equation for vortex field $\vec{X}$, that also spreads in space with the speed v. In case $\vec{X}(0, X_y, 0)$ and $X_y(x)$ we obtain

$$\frac{\partial^2 X_y}{\partial x^2} = \frac{1}{v^2}\frac{\partial^2 X_y}{\partial t^2} \quad (14)$$

that we can solve as,

$$X_y = X_{y0}e^{i(\omega t - kx)} \quad (15)$$

CONCLUSION

As seen from expressions (10) and (15) these two fields: the gravitational field $\vec{g}$ and the vortex field $\vec{X}$ create one other and spread in space by the velocity v, always remaining perpendicular to one another and to the spreading direction, similarly to the electric and magnetic fields in electromagnetic wave.

On the base of this model it is possible to explain the existence of black holes, dark energy and dark matter. Really, the destruction and a birth of stars always happen in space that is accompanied in changing of mass of these stars, in other words in changing of their gravitational fields. It was found that the universe is expanding (Hubble's law) at an increasing rate [5]. This means that in the considered constant volume of space the density of the universe decreases, what leads to the emergence of a new vortex field according to the formula (4). This field possesses a certain energy that can be evaluated approximately by Einstein's formula $\Delta W = c^2\Delta m$ [6].

The existence of this new field could be tested by the following simple experiment (Fig.1). Let us consider the interaction between two pellets: small of mass m and big of mass $M(t)$. The big pellet was filled by the water and this water begins to flow through the valve during a certain time. In equilibrium state we can write:

$$Tsin\alpha = G\frac{mM}{r^2} \quad (16)$$

$$Tcos\alpha = mg \quad (17)$$

As seen from figure 1 the mass of big pellet in the given time t can be written as:

$$M = M_0 - \rho\pi R^2 y \quad (18)$$

and $r = a - ltg\alpha$. By dividing equations (16) to the equation (17) we can found:

$$tg\alpha = \frac{GM}{g(a-ltg\alpha)^2} \quad (19)$$

or

$$g(a - ltg\alpha)^2 tg\alpha = G(M_0 - \rho\pi R^2 y) \quad (20)$$

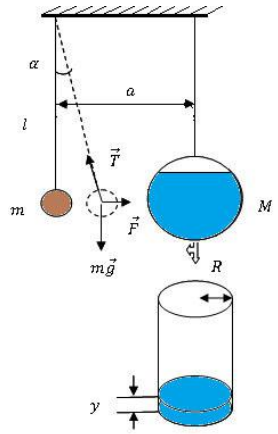

Fig. 1.

By measuring $\alpha(t)$ and $y(t)$ it is possible to test the validity of the equation (20). The deviation from expression (20) will mean the existence of a new vortex field.

In fact for exact estimation we must take into account a little shift of mass center of big pellet, that is negligible in the case, when $M \gg m$ and if the test is carried out in a short period of time.

[1] *Griffiths, David J.* (1998). Introduction to Electrodynamics (3rd ed.). Prentice Hall. p. 50. ISBN 0-13-805326-X.

[2] M J.C.axwell, 1881, A treatise on electricity and magnetism, Clarendon Press, Oxford, UK, 2nd Edition.

[3] Hazewinkel, Michiel, ed. (2001), "Maxwell equations", Encyclopedia of Mathematics, Springer, ISBN 978-1-55608-010-4

[4] *Sadiku, M. N. O.* (2007). Elements of Electromagnetics (fourth ed.). New York (USA)/Oxford (UK): Oxford University Press. p. 386.ISBN 0-19-530048-3.

[5] *A. Riess,; et al.* (September 1998). "Observational Evidence from Supernovae for an Accelerating Universe and a Cosmological Constant". The Astronomical Journal 116 (3): 1009–1038. arXiv:astroph/9805201. Bibcode:1998AJ....116.1009 R. doi:10.1086/300499.

[6] Max Jammer (1999), Concepts of mass in contemporary physics and philosophy, Princeton University Press, p. 51, ISBN 0-691-01017-X

Received: 17.10.2016

ADSORBENT REGENERATION BY ELECTRIC DISCHARGE INFLUENCE

A.M. GASHIMOV, K.M. GURBANOV, M.A. GASANOV, I.G. ZAKIYEVA, N.M. HOSSEINAHLI

Institute of Physics of Azerbaijan National Academy of Sciences
H.Javid ave., 131, AZ-1143, Baku, Azerbaijan
E-mail: arif@physics.ab.az, magerram-hasanov@rambler.ru

The adsorbent regeneration processes by electric gas discharge influence have been studied. The thermally stimulated relaxation method (TSR) widely used at study of electric charge relaxation in polymer films and other dielectric materials is used for revealing of charged state in natural adsorbents of benthonic clay. The influence of electric fields and discharges on natural adsorbent – bentonite leads to its additional regeneration and simultaneously to appearance of charged state in it.

Keywords: natural adsorbent, regeneration, torch discharge, monomer.
PACS: 52.25-b; 52.80. He; 52.00.00

INTRODUCTION

The main regularities taking place in the system "adsorbent – adsorbate – strong electric field" is necessary to reveal in the connection with big perceptivity of electric control of adsorption processes in problems of purification and liquid separation. The appearance of electric charges of different signs on the surface and in the adsorbent volume is the one of the essential physical factors defining the substance properties [1-4].

It is known that the influence of electric discharge on adsorbents changes their adsorptive capacity [5-7].

The adsorbents are treated by activating influences of different types for increase of efficiency: chemical, radiation, electric and etc. The influences by electric fields and discharges significantly changing the adsorptive capacity of adsorbents are the most effective ones.

The polarization processes in electric field or electric charge introduction directly on the surface or in material volume take place in the result of electric influences on adsorbents in them. The given processes lead to appearance of bound electric charges, i.e. the charged state in material forms [5-8]. As it is mentioned by authors of the given works, the electric charges introduced in adsorbent can be the centers of high adsorption from liquid of different impurities because of the Van-der-Waals force activity in system adsorbent – impurity particle.

The study of different mechanism changes in natural adsorbents treated by electric influences is necessary for solving of task of sorption process intensification with the help of electric discharges.

EXPERIMENT TECHNIQUE AND DISCUSSION OF OBTAINED RESULTS

The investigations of adsorbent regeneration process by influence of electric gas discharge have been carried out in the given paper.

Adsorbent-bentonite is treated by regeneration process in vacuum condition at 180ºC temperature; later the sample is divided into two parts each by 1300mg. Further, 350mg hydrocarbon composition monomer is added in ampoule with bentonite by height 1300mg and 82mg monomer is added in other one and both systems are endured during 24 hours.

The results characterizing the monomer adsorption process are presented in tables 1 and 2.

Table 1.

Monomer, 350 mg	
t, h	m, mg
1	340+1310
2	335+1315
5	330+1320
8	330+1320
24	330+1320

Table 2.

Monomer, 82 mg	
t, h	m, mg
1	72+1310
2	70+1312
5	66+1316
8	66+1316
24	66+1316

From tables 1 and 2 it is seen that adsorbent absorbs the insignificant monomer quantity and total saturation is observed during 5 hours. In further experiments the adsorbents saturated by monomer are treated by regeneration by the way of torch discharge influence in them. The principal electric scheme of material treatment by electric discharge of torch type is presented on fig.1.

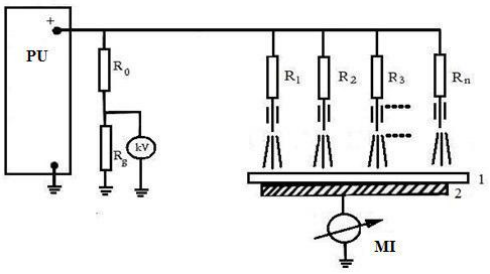

Fig.1. Principal electric scheme:
PU is power unit, kV is kilovolt-meter, R_0, R_g is resistance divisor, $R_1, R\ldots R_n$ are limiting resistors, MI is measuring instrument, 1 is metallic substrate, 2 is electrode.

131 H.Javid ave, AZ-1143, Baku
ANAS, G.M.Abdullayev Institute of Physics
E-mail: jophphysics@gmail.com

Further, the adsorption process is carried out again in previous conditions. The given process results are presented in tables 3 and 4.

The method of thermostimulated relaxation (TSR) widely used at study of electric charge relaxation in polymer films and other dielectric materials is used for revealing of charged state in natural adsorbents of bentonite clay [9].

The experiment of TSR method is carried out by the way of sample heating from room temperature up to 450ºC with constant velocity 2º/min with simultaneous record of relaxation current curve in temperature function (and time) on two-coordinate recorder with amplifier. The heating linearity is supplied by special electron device.

The thermostimulated current curve is shown on fig. 2. The presence of two high-temperature peaks (300ºC, 430ºC) proves the relaxation of electric charges in samples.

The square taken under current curve TSR in time function corresponds to sum charge relaxed in the sample. The charge quantity corresponded to peaks is: Q_1=1,8·10^{-7} coulomb; Q_2=2,8·10^{-7} coulomb.

Table 3.

Monomer, 350 mg	
t, h	m, mg
1	20+1630
2	12+1638
5	8+1642
8	6+1644
24	2+1648

Table 4.

Monomer, 82 mg	
t, h	m, mg
1	18+1364
2	12+1370
5	10+1372
8	8+1374
24	4+1378

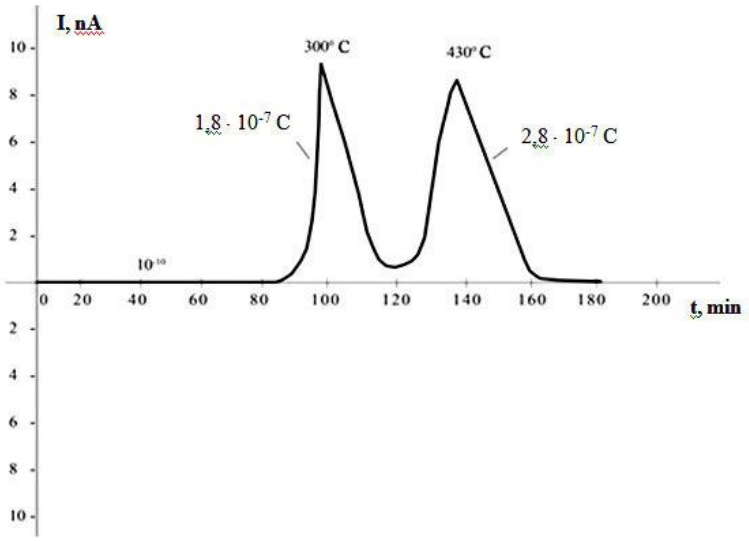

Fig. 2. The curve of thermostimulated current.

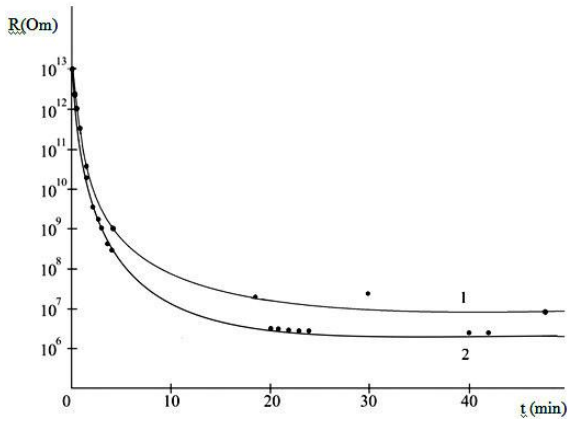

Fig.3. The dependence of bentonite electric resistance on degree of its saturation by steams before and after treatment by torch discharge:
1 is adsorbent nontreated by electric discharge
2 is adsorbent treated by electric discharge.

The results of carried investigations show that the adsorption ability of adsorbents increases in many times at their regeneration with torch discharge influence. The fact of increase of bentonite adsorption ability is proved again in further experiments. The bentonite treated by the influence of torch discharge is used in bentonite. The change of adsorbent resistance fig.3) in dependence on humidification degree before and after treatment is investigated.

The bentonite humidification is carried out by two methods: by the way of water barbotage and also by aging of bentonite portion in atmosphere with humidity 50%. Moreover, the mass change and sample electric resistance are mentioned in definite time periods. The quantity of absorbed water is defined by mass change.

The bentonite intensively adsorbs the steams and in time (approximately after 40 hours) the process transforms into saturation region in initial stages. The measurement of electric resistance through the definite time intervals correspondent to definite humidification degrees allows us to reveal the dependence character of specific resistance change on humidity time (fig.3).

CONCLUSION

Thus, it is shown that the influence of electric fields and discharges on natural adsorbent-bentonite leads to its additional regeneration. This is connected with the fact that the bound water in adsorbent transforms into dissolved state under influence of electric discharge on adsorbent and it easily desorbs. The electro-treatment of adsorbents makes wider the bentonite application in different technological processes.

[1] *M.A. Yegorov.* Voda: ximiya I ekoloqiya. 2008, n.4, s. 41-43. (in Russian).
[2] *Sh. Wang, Y. Peng*. Chemical Engineering Journal. 2010, vol. 156, Issue 1, 11-24.
[3] *A.S. Shilina, V.K. Milinchuk*. Sorbtsionnie i khromatograficheskie protsessi, 2010, t.10, vip. 2, s. 237-245.
[4] *E.S. Klimov, M.V. Buzayeva*. Prirodnie sorbenti i kompleksoni v ochistke stochnikh vod. Ulyanovsk Ul GTU, 2011. 201 s.
[5] *A.M. Gashimov, V.A. Aliyev, K.B. Gurbanov, M.A. Gasanov.* Fizika i khimiya obrabotki materialov, Moskva, 2005, n. 2, s. 86-89.
[6] *M.A. Gasanov.* Fizika i khimiya obrabotki materialov, Moskva, 2006, n. 5, s.88-91.
[7] *A.M. Gashimov*, *M.A. Gasanov.* Elektronnaya obrabotka materialov. 2008, n. 6, s. 46-51.
[8] *A.M. Gashimov*, *M.A. Gasanov.* Jurnal Fizicheskoy khimii, 2009, t. 83, n.7, s. 1352-1355.
[9] *G. Sesler.* Elektreti. M.: Mir, 1983, 488 s.

Received: 14.07.2016

ISSN 1028-8546

2016, Vol. XXII, № 4
Section: En

CONTENTS